

Cite this: *Phys. Chem. Chem. Phys.*, 2012, **14**, 14982–14998

www.rsc.org/pccp

PERSPECTIVE

## Applications of light scattering in dye-sensitized solar cells

Qifeng Zhang,<sup>a</sup> Daniel Myers,<sup>a</sup> Jolin Lan,<sup>a</sup> Samson A. Jenekhe<sup>bc</sup> and Guozhong Cao<sup>\*ab</sup>

Received 4th September 2012, Accepted 4th September 2012

DOI: 10.1039/c2cp43089d

Light scattering is a method that has been employed in dye-sensitized solar cells for optical absorption enhancement. In conventional dye-sensitized solar cells, large TiO<sub>2</sub> particles with sizes comparable to the wavelength of visible light are used as scatterers by either being mixed into the nanocrystalline film to generate light scattering or forming a scattering layer on the top of the nanocrystalline film to reflect the incident light, with the aim to extend the traveling distance of incident light within the photoelectrode film. Recently, hierarchical nanostructures, for example nanocrystallite aggregates (among others), have been applied to dye-sensitized solar cells. When used to form a photoelectrode film, these hierarchical nanostructures have demonstrated a dual function: providing large specific surface area; and generating light scattering. Some other merits, such as the capability to enhance electron transport, have been also observed on the hierarchically structured photoelectrode films. Hierarchical nanostructures possessing an architecture that may provide sufficient internal surface area for dye adsorption and meanwhile may generate highly effective light scattering, make them able to create photoelectrode films with optical absorption significantly more efficient than the dispersed nanoparticles used in conventional dye-sensitized solar cells. This allows reduction of the thickness of the photoelectrode film and thus lowering of the charge recombination in dye-sensitized solar cells, making it possible to increase further the efficiency of existing dye-sensitized solar cells.

### 1. Introduction

Solar cells are a type of device based on the photovoltaic effect to convert solar energy to electricity.<sup>1</sup> So far, the development of solar cells has undergone three generations. First generation solar cells are built on V or II–VI group single crystal

<sup>a</sup> Department of Materials Science and Engineering, University of Washington, Seattle, WA 98195, USA

<sup>b</sup> Department of Chemical Engineering, University of Washington, Seattle, WA 98195, USA

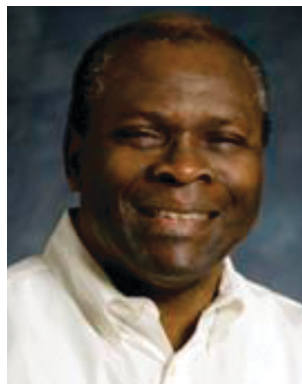
<sup>c</sup> Department of Chemistry, University of Washington, Seattle, WA 98195, USA. E-mail: gzc@u.washington.edu



Qifeng Zhang

Qifeng Zhang earned his PhD degree from Peking University. Currently he is Research Assistant Professor in the Department of Materials Science and Engineering at University of Washington. His research interests involve engineering nano-structured materials for applications to electrical devices, including solar cells, UV light-emitting diodes (LEDs), field-effect transistors (FETs), and gas sensors. His current research is focused on dye-sensitized

solar cells (DSCs), Cu<sub>2</sub>ZnSnS<sub>4</sub> (CZTS)-based thin film solar cells, quantum dot solar cells, and organic/inorganic hybrid solar cells.



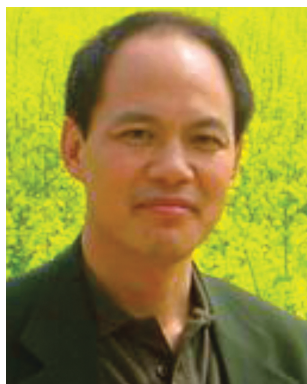
Samson A. Jenekhe

Samson A. Jenekhe received his BS degree from Michigan Technological University in 1977 and PhD degree from University of Minnesota in 1985. He is currently Boeing-Martin Professor of Chemical Engineering and Professor of Chemistry in the Department of Chemical Engineering at University of Washington. His research interests involve: (1) organic electronics and optoelectronics, including thin film transistors, solar cells, and LEDs; (2) self-assembly

and nanotechnology, including block copolymers, nanowires, and multicomponent self-assembly; and (3) polymer science, including synthesis, processing, properties, and photonic applications.

semiconductors, with which a bulk p–n junction is established to separate photogenerated electron–hole pairs. The theoretical limit to the efficiency of single junction solar cells based on these materials is about 31%.<sup>2</sup> Currently, the first generation solar cells are most represented in commercial production, with about 90% of the current market share. The second generation is also derived mainly from the V or II–VI group semiconductor materials, however, with the consideration of lowering costs. Owing to the development of vacuum deposition technology, the devices have been developed using thin films so as to reduce the material mass and thus lowering the costs. The second generation solar cells feature conversion efficiencies typically in a range of 18–20%. Although such conversion efficiencies have been able to meet the requirements for most uses in low power electrical appliances, the costs of the materials and of manufacturing are still somewhat too high and therefore limit practical application of these cells.

The high cost of the first and second generation solar cells has motivated the development of third generation solar cells based on new materials, structures and concepts. The third generation solar cells are represented by *polymer-based organic solar cells* and *Grätzel-type dye-sensitized solar cells* (DSCs). These solar cells feature relatively low production costs while providing decent conversion efficiencies that may be satisfactory for practical applications. Comparing these two kinds of solar cells, the polymer-based organic solar cells are thought to have great potential due to the diversity of polymers available through molecular design, which potentially allows the creation of a highly efficient p–n junction and thus deliver very high efficiency solar cells. Recently, the record efficiencies of ~6% for single-layer polymer solar cells and 8.62% for tandem polymer solar cells have been announced.<sup>3</sup> However, the lack of chemical stability of the polymer materials is still a problem for the polymer solar cells, which must be exposed to long term sunlight under ambient conditions. Being so far superior to polymer solar cells, DSCs have been able to provide conversion efficiencies as high as 11–12%,<sup>4,5</sup> and the lifetime of DSCs has been demonstrated as even longer than 20 years in operating condition, with only a slight degradation of the dye materials.<sup>4</sup>



**Guozhong Cao**

*Guozhong Cao is Boeing-Steiner Professor of Materials Science and Engineering, Professor of Chemical Engineering, and Adjunct Professor of Mechanical Engineering at University of Washington. He received his PhD degree from Eindhoven University of Technology, MS from Shanghai Institute of Ceramics of Chinese Academy of Sciences and BS from East China University of Science and Technology. His current research is focused mainly on*

*chemical processing of nanomaterials for energy related applications including solar cells, lithium-ion batteries, supercapacitors, and hydrogen storage.*

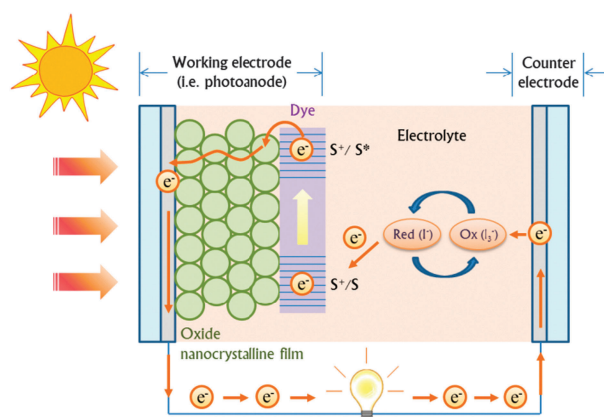


**Fig. 1** Structure and operating mechanism of a dye-sensitized solar cell.

In addition, the very low cost in materials and ease of manufacturing are also the reasons that make the DSCs still attractive nowadays.

DSCs are in essence a photoelectrochemical system<sup>6,7</sup> as shown in Fig. 1, in which one of the electrodes, the so-called photoanode or working electrode, is made of a layer of a 10 to 15  $\mu\text{m}$ -thick oxide film sensitized by dye molecules fabricated on a glass substrate coated with a transparent conductive film, and the other electrode, the so-called counter electrode, is a glass or silicon substrate coated with a platinum film. These two electrodes are separated by  $\sim 40$   $\mu\text{m}$ -thick spacers, and a liquid electrolyte that contains  $\text{I}^-/\text{I}_3^-$  redox couples is introduced into the space between the two electrodes as a conductive medium. The light irradiating from the photoanode side is captured by the dye molecules that are adsorbed on the oxide, leading to the generation of photoexcited electrons in the dye molecules. The photogenerated electrons then transfer into the oxide, diffuse in the oxide, and are finally collected by the transparent conductive film on the glass substrate, which is connected to external circuit. The photo-oxidized dye molecules are reduced by electrons provided by  $\text{I}^-/\text{I}_3^-$  redox couples in the electrolyte. Those photogenerated electrons at the photoanode travel through the external circuit, reach the platinum-coated counter electrode and, finally, gain access to the electrolyte, reducing the  $\text{I}^-/\text{I}_3^-$  redox couples and enabling the electrolyte to be regenerated. In DSCs, the optical absorption as well as the generation of photoelectrons is performed by the dye molecules, while the charge transport occurs within the oxide semiconductor. These two processes are linked by a process of electron transfer from the dye molecules to the oxide semiconductor, owing to the long decay time of the photoexcited electrons in the lowest unoccupied molecular orbital (LUMO) level of the dye molecules and a difference in the energy levels between the dye and oxide. Based on such a photovoltaic mechanism, to improve the conversion efficiency of a DSC, on one hand, one can either use dye molecules with a higher absorption coefficient and an extended long-wavelength absorption edge or increase the internal surface of the photoelectrode film for more dye adsorption to enhance optical absorption of the photoelectrode.<sup>8</sup> On the other hand, one can employ one-dimensional nanostructures to provide a direct path for electron diffusion and thus promote charge transport, or develop new sensitizers or electrolytes to

reduce the recombination in DSCs.<sup>9–11</sup> In addition to the aforementioned ways of improving DSC performance, light scattering is another important method that has been adopted to enhance the conversion efficiency of DSCs.<sup>12</sup> The basic idea of a light scattering method is to confine the light propagation and extend the traveling distance of light within the photoelectrode film so as to increase the opportunity of the photons to be absorbed by the dye molecules, and in this way, to enhance the light harvesting efficiency of the photoelectrode as well as the conversion efficiency of the solar cells.

This paper reviews the applications of light scattering in DSCs over the past two decades and some recent progress in this topic. It will show that, conventionally, the light scattering can be generated by introducing submicron-sized large particles into nanocrystalline films, which serve as the basic absorbing layer in traditional DSCs. The large particles as light scatterers may either be embedded into the nanocrystalline film to form a mixed structure photoelectrode film, or be applied onto the nanocrystalline film to form a light scattering layer and result in a double-layer structure photoelectrode film. Besides the use of large particles combined with nanocrystalline films, recently a class of hierarchical nanostructure consisting of nano-sized oxide crystallites assembled into spherical aggregates has been developed for application in DSCs, with particular emphasis on providing a large surface area and generating light scattering simultaneously so as to overcome the drawback of conventional methods using large particles for light scattering, in which the large particles unavoidably lead to a loss of internal surface area of the photoelectrode film in the case of mixed structures, or the incident light is only reflected once with the double-layer structure.<sup>13,14</sup> Through using a photoelectrode film constructed with hierarchical nanostructure called nanocrystallite aggregates, the Cao group has gained a more than 140% increase in the conversion efficiency of ZnO-based DSCs.<sup>15,16</sup> In the outlook section, hierarchical nanostructures are emphasized as promising materials for achieving high efficiency DSCs in view of their dual function in providing a large surface area and generating effective light scattering, which allows a reduction in the thickness of the photoelectrode film and therefore a decrease in the rate of charge recombination. While the focus of this paper is on a review of technical issues regarding the utilization of light scattering effects in DSCs to enhance the optical absorption, it is expected that this paper may also convey insight about how the materials can be tailored to benefit solar cells in terms of light harvesting and electron transport.

## 2. Light scattering theory

Light scattering is a common phenomenon in optics regarding the propagation of light in the presence of object(s). Normally, when light encounters an object, according to the laws of reflection and refraction, the radiation may either propagate in the forward direction, giving rise to *refraction* and *absorption*, or propagate in the backward direction, causing *reflection*, as shown in Fig. 2a. However, under certain condition when the dimensions of the object are on the order of the wavelength of light, the radiation will be spread in all directions that deviate

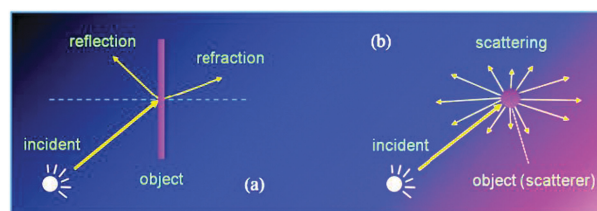


Fig. 2 Reflection, refraction and scattering of light.

from the trajectory of the reflected or refracted light as determined by the laws of reflection and refraction, as shown in Fig. 2b. Such an optical phenomenon is called light scattering, and the object that causes the light scattering is known as the *scatterer* or *scattering center*.<sup>17–19</sup>

Many theories have been developed to describe the process of light scattering. Among them, Rayleigh scattering theory and Mie scattering theory are typically applicable for spherical scatterers such as particles, droplets, and density fluctuations. These two theories are categorized according to the comparability between the light wavelengths and the feature size of the scatterers. Specifically, the theory of Rayleigh scattering describes dielectric (non-absorbing) scatterers with a small size. The criteria for Rayleigh scattering are  $\alpha \ll 1$  and  $|m|\alpha \ll 1$ , where  $\alpha = 2\pi r/\lambda$ ,  $r$  is the scatterer radius,  $\lambda$  is the wavelength of the incident light, and  $m$  is the refractive index of the scatterer defined as  $m = n - ik$  ( $n$  indicates the refraction of light and the complex term,  $k$ , is related to absorption). Based on such criteria, the Rayleigh scattering theory is applicable for describing the light scattering caused by the scatterers with characteristic dimensions much smaller than the wavelength of incident light. In the region of Rayleigh scattering, the intensity of the light scattered by a single particle can be readily calculated with the following equation<sup>17</sup>

$$I = I_0 \frac{1 + \cos^2 \theta}{2d^2} \left( \frac{2\pi}{\lambda} \right)^4 \left| \frac{m^2 - 1}{m^2 + 2} \right|^2 r^6 \quad (1)$$

where  $I_0$  is the incident intensity,  $d$  is the distance to the particle, and  $\theta$  is the scattering angle. By integrating over the sphere surrounding the particle, the Rayleigh scattering cross section,  $\sigma_{\text{scat, Rayleigh}}$ , can be given as

$$\sigma_{\text{scat, Rayleigh}} = \frac{2\pi^5}{3} \frac{(2r)^6}{\lambda^4} \left| \frac{m^2 - 1}{m^2 + 2} \right|^2 \quad (2)$$

From eqn (2), it can be seen that the Rayleigh scattering cross sections are proportional to the 6th power of particle size, and inversely proportional to the 4th power of wavelength. This has been used to explain the blue color of our sky, as the air molecules (*e.g.*  $\text{N}_2$  and  $\text{O}_2$ ) are well within the Rayleigh regime so that the shorter blue light of the sun can be scattered more efficiently than the longer red light.

In another case where the scattering system consists of large particles, *i.e.* the size of the particles is comparable to the wavelength of the incident light, Mie scattering theory is the only theoretical description is applicable. Note that the Mie scattering theory has no limitations to the particle size and can be used for scattering systems composed of spherical particles regardless of whether the particles is of a light absorbing or

non-absorbing material. The cross section of Mie scattering is given by the expression

$$\sigma_{\text{scat, Mie}} = \frac{\lambda^2}{2\pi} \sum_{n=0}^{\infty} (2n+1)(|a_n|^2 + |b_n|^2) \quad (3)$$

where the parameters  $a_n$  and  $b_n$  are defined by the Riccati-Bessel functions  $\Psi$  and  $\xi$  as

$$a_n = \frac{\Psi_n(\alpha)\Psi'_n(m\alpha) - m\Psi_n(m\alpha)\Psi'_n(\alpha)}{\xi(\alpha)\Psi'_n(m\alpha) - m\Psi_n(m\alpha)\xi'_n(\alpha)} \quad (4)$$

$$b_n = \frac{m\Psi_n(\alpha)\Psi'_n(m\alpha) - \Psi_n(m\alpha)\Psi'_n(\alpha)}{m\xi(\alpha)\Psi'_n(m\alpha) - \Psi_n(m\alpha)\xi'_n(\alpha)} \quad (5)$$

Accordingly, the Mie scattering efficiency,  $Q_{\text{scat, Mie}}$ , can be calculated by

$$Q_{\text{scat, Mie}} = \frac{\sigma_{\text{scat, Mie}}}{\pi r^2} \quad (6)$$

With these equations, the dependence of the Mie scattering efficiency on particle size and incident wavelength can be calculated. Shown in Fig. 3 is an example of calculation for scatterer being a sphere of  $\text{TiO}_2$  material in air. From Fig. 3a where the wavelength of incident light is set to 532 nm, it can be seen that an effective light scattering can only take place when the size of spherical scatterer is larger than 200 nm in diameter – approximately half of the wavelength of incident light. The relation between the wavelength of incident light and the particle size can be further demonstrated by a calculation of the dependence of scattering efficiency on the wavelength of incident light for a spherical scatterer with fixed diameter. The result shown in Fig. 3b is an example for 200 nm spherical scatterer, exhibiting that the light scattering mainly occurs in the wavelength range from  $\sim 400$  nm to  $\sim 650$  nm. One can therefore draw a rough conclusion from these calculations that, to achieve an effective light scattering, it is expected that the size of the scatterer is comparable to the wavelength of the incident light. (Note that there would be a shift for the effectual range of the scatterer's size in the case of a practical DSC system, in view of the refractive index being different for air and iodide electrolyte; the latter being an electrolyte that is most widely used in DSCs.) In fact, such a prediction in theory has been the criterion for determining the size of particles used in the photoelectrode film of DSCs for the generation of light

scattering aimed at improving the optical absorption of the photoelectrode, although the Mie scattering theory is generally applicable to a single scattering or a system including sufficiently separated scatterers, which is not completely the same as practical photoelectrode films typically consisting of particles that are closely packed.

### 3. Applications of light scattering in DSCs

Light scattering has been applied to DSCs in the hope of enhancing optical absorption of the photoelectrode film. In general, there are two approaches that have been conventionally adopted to introduce light scattering into the photoelectrode film of a DSC. One so-called *mixture structure* is where large particles with a size comparable to the wavelength of light are embedded into a nanocrystalline film, which consists of nano-sized crystallites forming the basic absorbing layer of the DSCs. The large particles embedded into the nanocrystalline film act as light scatterers to generate multiple light scattering and as such extend the travelling distance of light within the photoelectrode film, leading to an increase in the probability of photons to be absorbed. The second method, the so-called *double-layer structure* is where the large particles are placed on the top of the nanocrystalline film to form a light scattering layer, so that the incident light can be reflected back to the film, resulting in more absorption. In both of these structures, the nanocrystalline film functions as the primary absorber to provide a sufficient surface area for dye adsorption, while the large-size particles which are introduced to generate light scattering will however unavoidably cause a loss of internal surface area of the photoelectrode film in the case of a mixed structure, or increase the internal resistance of the solar cells and hinder charge transport within the solar cells in the case of a double-layer structure. Obviously, there is a necessity for theoretical analysis to optimize the microstructure of photoelectrode films so as to maximize the effect of light scattering on the enhancement of DSCs' performance.

#### 3.1 Theoretical prediction

Quite a few theoretical works have been reported the design and optimization of the structure of DSC photoelectrodes integrated with a light scattering function.<sup>22,24–26</sup> An impressive study performed by Ferber *et al.* investigated the influence of

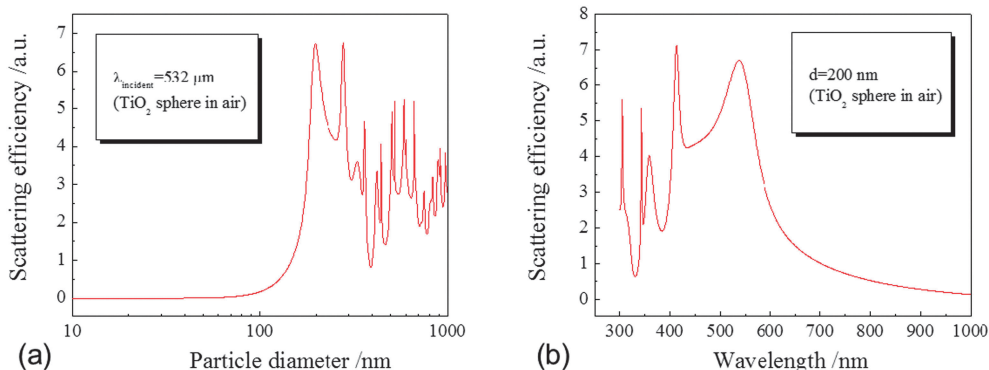


**Fig. 3** The dependences of scattering efficiency on (a) particle size and (b) incident wavelength. (The calculation is based on a  $\text{TiO}_2$  sphere in a surrounding medium of air. Refractive indices of  $\text{TiO}_2$  are obtained from ref. 20 and 21).

size and concentration of light scatterers and the structure of the photoelectrode film on optical absorption of the photoelectrode *via* computer simulation.<sup>22</sup> The simulation was based on a model in which the photoelectrode film was either consisted of TiO<sub>2</sub> nanoparticles in a diameter of 20 nm mixed with large-sized TiO<sub>2</sub> particles to form a binary particle mixture, or included a layer of 20 nm sized TiO<sub>2</sub> nanoparticles combined with another layer of large-sized particles for backward scattering. The particles were assumed to be covered with a monolayer of dye molecules. According to Mie theory in the case of coated sphere scatterers, multiple scattering was calculated using a numerical solution of the radiative transfer equation. The result of the calculation revealed that only the particles with sizes in the range of the wavelength of light were effective in generating light scattering, whereas the scattering of 10–25 nm sized TiO<sub>2</sub> nanoparticles was so small as to be negligible. The simulation also illustrated that, for the film with mono-sized nanocrystalline particles, optical absorption reached a maximum when the internal surface was largest. This can be easily understood in view of the fact that, in DSCs, the absorption was predominated by dye molecules that are adsorbed on the oxide and therefore, a larger internal surface would be able to hold more dye molecules. For the photoelectrode film with a mixed structure, the simulation indicated an appreciable decrease in the internal surface due to the addition of large-sized particles. However the simulation predicted that the optical absorption of the photoelectrode was ultimately enhanced owing to the light scattering. An optimal structure to the photoelectrode film was proposed as a mixture containing 5 wt% large particles with radius 125–150 nm and 95 wt% nanocrystalline particles in 20 nm size, giving rise to the maximal increase in optical absorbance, as shown in Fig. 4. The simulation also predicted that too many large-sized particles mixed into the nanocrystalline film might, on one hand greatly lower the effective internal surface area and, on the other hand, cause too much back-scattering, resulting in an unwanted increase in the reflectance instead of an increase in the absorbance of the photoelectrode film. According to the simulation done by Ferber *et al.*, a double-layer structure photoelectrode comprised of a nanocrystalline film and a back-surface scattering layer

with large-sized particles was not recommended, in view of the simulated result showing that the optical absorbance of a double-layer structure photoelectrode was not better than that of the mixture structure photoelectrode. Moreover, from the ease-of-manufacture point of view, there was much extra work to prepare a multilayer structured electrode.

It is worth pointing out that, since the Mie scattering is best applicable to single scattering, the simulation of multiple scattering done by Ferber *et al.* was therefore set to be based on a particle system with the volume fraction of the scatterers being as low as 10–30%, so as to ensure the scatterers were sufficiently separated and thus there was no need to account for phase effects during the simulation. However, it should be realized that such a 10–30% volume fraction is much lower than that of ~50% in a conventional DSC photoelectrode film consisting of sintered nanoparticles and, therefore, the simulation result may not be able to completely reflect the practical effect of light scattering in a system constituting a nanocrystalline film mixed with large-sized particles. For example, the incorporation of large-sized particles into a nanocrystalline film may unavoidably cause a decrease in the internal surface area of the photoelectrode film. This would lower the adsorption amount of dye and therefore, to some degree, counterbalance the optical absorption enhancement due to light scattering. However, according to the simulation, the optical absorption enhancement in a binary mixture structure photoelectrode was found to be at the same level as that in a double-layer structure photoelectrode. Nevertheless, a qualitative prediction to achieving the maximum efficiency through a use of certain-sized large particles (*e.g.*, 250–300 nm in diameter) mixed into nanocrystalline film in a certain percentage (*e.g.*, 5 wt%) remains valid. Another theoretical study using a four-flux radiative transfer calculation done by Vargas *et al.* predicted that, in addition to the size of the scatterers, the maximum value of effective scattering coefficient was also correlated to the volume fraction of the scatterers.<sup>28</sup> According to the calculation, for TiO<sub>2</sub> particle scatterers ~250 nm in diameter, the maximum effective scattering coefficient could be reached when the volume fraction was 25%.

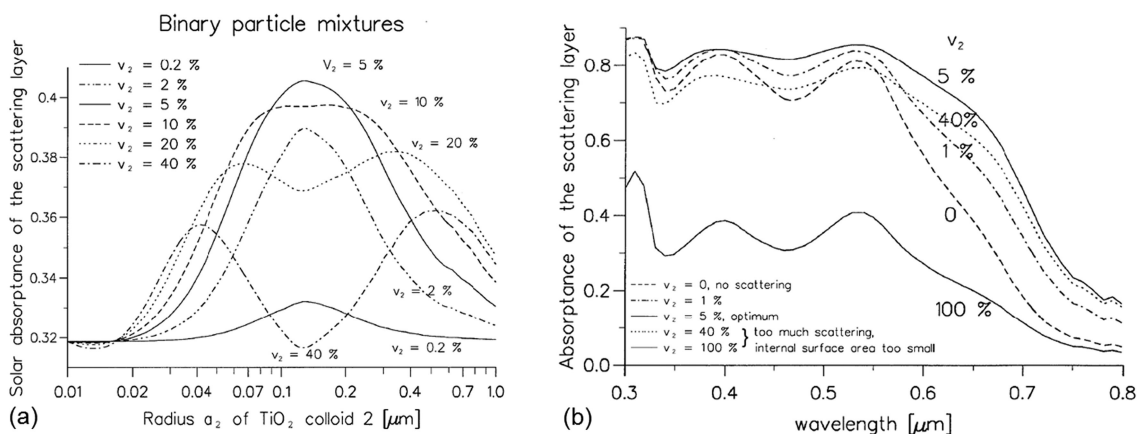


**Fig. 4** Calculated solar absorbance as a function of (a) the radius of scatterers (*i.e.*, large-sized particles), and (b) the wavelength of incident light. The films are 10  $\mu\text{m}$  in thickness and formed by binary mixture of nanocrystalline TiO<sub>2</sub> particles (10 nm in radius) with weight fraction  $v_1$  and large-sized particles with radius of  $a_2$  and weight fraction  $v_2 = 1 - v_1$ . In (b) the large-sized particles are 135 nm in radius.<sup>22</sup>

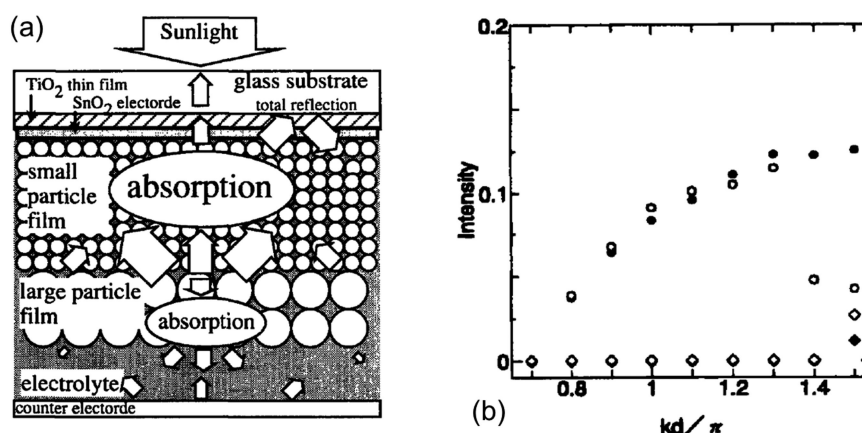


**Fig. 5** A proposed multilayer structure DSC photoelectrode with a light scattering layer. (a) Schematic drawing of the structure of the photoelectrode including a layer of large-sized  $\text{TiO}_2$  particles for light scattering, a layer of small particles for dye adsorption, and a thin film of  $\text{TiO}_2$  placed between the glass substrate and nanocrystalline film for total reflection, and (b) calculated dependence of light scattering intensity on scatterer size, where  $k$  is the wavenumber of incident light, and  $d$  is the diameter of scatterers.<sup>23</sup>

Using the theoretical model same as what was adopted by Ferber *et al.*, Usami also performed a systematic theoretical study regarding the light scattering effect in DSC photoelectrode films with a multiple-layer structure, with the aim of enhancing optical confinement by including an extra layer for light reflection.<sup>23</sup> Based on the computer simulation results, it was proposed that an optimal DSC photoelectrode film should be a three layer structure that consisted of a layer of conventional  $\text{TiO}_2$  nanocrystalline film, a layer of large-sized  $\text{TiO}_2$  particles deposited on the top of the nanocrystalline film for light scattering, and a thin layer of rutile  $\text{TiO}_2$  film inserted between the nanocrystalline film and the glass substrate for total reflection to the scattered light, as shown in Fig. 5a. It was emphasized that such a structure allowed the light to be confined and therefore absorbed highly effectively because of multiple reflection of light between the scattering layer and the total reflection layer. In this simulation, an optimal diameter of the large  $\text{TiO}_2$  particles for light scattering was predicted to be  $\sim 1.3\text{--}1.4 \times \pi/k$ , where  $k$  was the wavenumber of the incident light (Fig. 5b). When this condition was satisfied, it was predicted that the backscattered intensity could reach a maximum. As a result of the multiple-layer structure that might yield optical confinement, the multiple-layer structure photoelectrode was found to be able to achieve much greater optical absorption enhancement than the mixed structure.<sup>29</sup> These theoretical works well exemplify that the performance of DSCs is closely related to the structure of photoelectrode film, which may affect the light propagation to a large extent and thus influence the optical absorption of the photoelectrode. A careful design of the structure of photoelectrode film may allow the use of optical effects to enhance the optical absorption of the photoelectrode, so as to achieve high-efficiency DSCs.

## 3.2 Practical applications

### 3.2.1 Mixture structure

(1) *Large  $\text{TiO}_2$  particles as light scatterers.* The consideration of using large particles in DSCs for light scattering originates from one of Grätzel's works, in which it was found that  $\text{TiO}_2$  films consisting of nanoparticles prepared with a

hydrothermal method at a temperature of  $250\text{ }^\circ\text{C}$  were translucent in color and presented a higher DSC conversion efficiency than the films consisting of nanoparticles synthesized at relatively low temperatures (for example, below  $230\text{ }^\circ\text{C}$ ).<sup>27</sup> The latter, *i.e.* the films with nanoparticles synthesized at low temperatures, were fully transparent. It was suggested that there was an agglomeration of nanoparticles in the films with the nanoparticles autoclaved at  $250\text{ }^\circ\text{C}$ . The agglomeration of nanoparticles resulted in light scattering and thus enhanced optical absorption of the photoelectrode in near-infrared region around  $700\text{ nm}$  wavelength where the ruthenium-based metal-organic dyes, known as N3, N719 and "black dye" were not thought very efficient. However, although the photoelectrode film including the agglomeration of nanoparticles might lead to an improvement in the solar cell efficiency, the nanoparticles autoclaved at  $250\text{ }^\circ\text{C}$  contained a portion (up to 30 wt%) of rutile  $\text{TiO}_2$ . The rutile nanoparticles were photoactive at wavelengths below  $\sim 400\text{ nm}$ , therefore causing a problem with long-term stability of the solar cells. To avoid the inclusion of rutile in the photoelectrode film while retaining the light scattering effect, an alternative way was proposed to use nanoparticles with pure anatase which were autoclaved at a relatively low temperature, for example  $230\text{ }^\circ\text{C}$ , and including large  $\text{TiO}_2$  particles mixed into the nanoparticle film for the generation of light scattering. To this end, Fluka  $\text{TiO}_2$  particles, which are commercially available and feature a size distribution centered at  $\sim 300\text{ nm}$ , were employed by Barbe *et al.* to generate purposely light scattering in the DSCs for the first time. It was demonstrated that an optimum composition for the photoelectrode film to gain the maximal enhancement in optical absorption caused by light scattering was 85% nanocrystalline particles mixed with 15% of Fluka particles. Fig. 6 presents a comparison between the specular/diffuse transmission and reflection spectra of a nanocrystalline film and the spectra of a nanocrystalline film mixed with 15% Fluka particles, showing a greatly increased diffuse transmission, however an apparently decreased specular transmission in the wavelength region above  $600\text{ nm}$  due to the light scattering generated by Fluka particles.

Another impressive work regarding the use of large  $\text{TiO}_2$  particles as light scatterers in a mixed structure photoelectrode

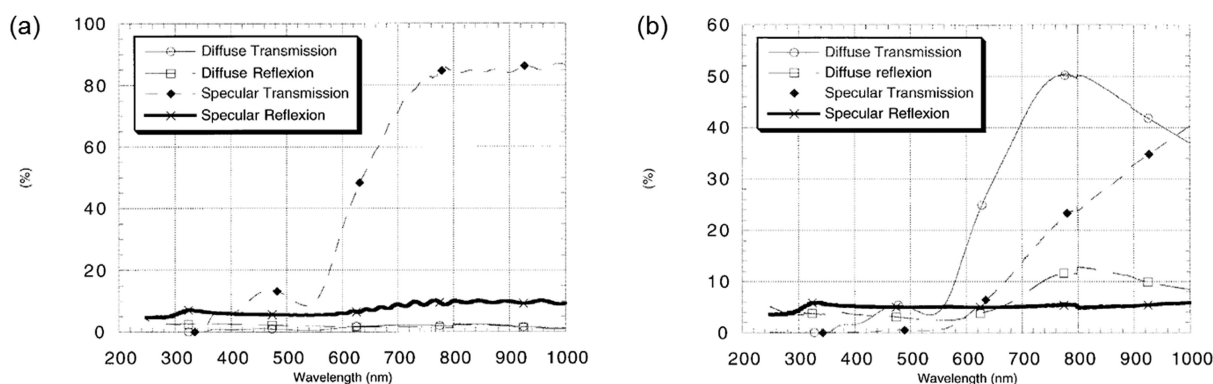


**Fig. 6** Transmittance and reflectance spectra of photoelectrodes with (a) a nanocrystalline film, and (b) a nanocrystalline film incorporated with 15% Fluka particles.<sup>27</sup>

was reported by Wang *et al.* using TiO<sub>2</sub> particles with 100 nm diameter synthesized with a hydrolysis method.<sup>30</sup> Convincing evidence found in this work that supports the light scattering enhancement effect is that, as expected, although the dye adsorption of  $1.59 \times 10^{-7}$  mol cm<sup>-2</sup> for a photoelectrode film containing nanocrystalline particles mixed with large particles at a ratio of 6 : 4 was lower than that of  $2.59 \times 10^{-7}$  mol cm<sup>-2</sup> for the film that only consisted of nanocrystalline particles, for the reason that the inclusion of large-sized particles resulted in the loss of internal surface area of photoelectrode film, the film that contained large particles presented a short-circuit current density of 15.65 mA cm<sup>-2</sup> and power conversion efficiency of ~8.37%, higher than the 14.86 mA cm<sup>-2</sup> and ~7.62% for the film made of nanocrystalline particles alone. Such a scenario demonstrated well that mixing large TiO<sub>2</sub> particles into a nanocrystalline film was an effective way to generate light scattering and thus to contribute to the enhancement of optical absorption as well as the photocurrent of a DSC. An investigation of incident-photon-to-current efficiency (IPCE) spectra carried out by Wang *et al.* further revealed that the light scattering benefited the solar cells by enhancing the optical absorption of photoelectrode mainly in the wavelength region greater than 600 nm. Kang *et al.* also reported such a red-shift phenomenon with respect to optical absorption due to light scattering observed on a solid-state DSC, in which the photoelectrode film was comprised of nanocrystalline particles mixed with 10 wt% light scattering particles.<sup>31</sup>

While the scattering efficiency is thought to be determined predominantly by the size of the TiO<sub>2</sub> particle scatterers, it was found that the surface roughness of the particles might also have an influence on the effectiveness of light scattering. Yang *et al.* observed that a film consisting of rough TiO<sub>2</sub> spheres (~275 nm in diameter) presented an apparently higher diffuse reflectance than a film consisting of smooth TiO<sub>2</sub> spheres, meaning more efficient light scattering capability of the TiO<sub>2</sub> particles with rougher surface.<sup>32</sup> However, the effectiveness of a rough surface on the light scattering enhancement still remains debatable. Theoretical studies reveal that the surface roughness affects light scattering in complex ways and the enhancement can be achieved depending on multiple factors such as the particle size, the microstructure of the particle surface, the wavelength of incident light, and so forth.<sup>33,34</sup> Besides the enhancement in light scattering, another merit of

the particle scatterers with rough surface while being used for DSCs is to achieve more dye loading than smooth ones.

In general, using large particles mixed into the nanocrystalline film is a simple way of generating light scattering so as to improve the optical absorption of DSCs. Compared with the double-layer structure, one of the obvious advantages of the mixed structure is its ease of manufacture.<sup>35</sup> However, the fact that the large particles mixed into the nanocrystalline film lead to a decrease in the internal surface area of the photoelectrode film is a drawback of this method, which limits the light scattering enhancement effect to a certain extent.

(2) *Spherical voids as light scatterers.* Spherical voids, a kind of hollow structure purposely introduced into nanocrystalline films, can also be employed as light scattering centers for DSCs. To fabricate spherical voids in a nanocrystalline film, according to the method described by Hore *et al.*,<sup>36</sup> polystyrene spheres with radius of 200 nm was mixed with TiO<sub>2</sub> colloidal paste in a ratio of 1 : 5 by volume. The film prepared with the mixed paste was annealed at 450 °C to burn out the polystyrene particles and leave spherical voids in the film (Fig. 7a and b). With a model of electrolyte-filled spherical voids surrounded by a medium of TiO<sub>2</sub> and using Mie theory, the optimal sizes of the voids were determined to be in the range of 50–100 nm, giving rise to the most intensive light scattering. Shown in Fig. 7c is a comparison between the diffuse reflectance spectra of the nanocrystalline films without and with spherical voids, implying that the embedded voids are quite effective in generating light scattering. One test of the spherical voids as light scatterers in DSCs had resulted in a 25% improvement in the conversion efficiency. In addition to playing a role in generating light scattering, the spherical voids with a hollow structure had been also demonstrated the advantage of allowing the liquid electrolyte to permeate into the nanocrystalline film, making it possible to use an electrolyte with high viscosity or low ion diffusion constant in DSCs.<sup>36</sup> Besides the polystyrene spheres, carbon spheres produced with a hydrothermal method by hydrolyzing glucose have been also studied to act as a template for the creation of spherical voids in a TiO<sub>2</sub> nanocrystalline film, demonstrating the highest efficiency of 7.2% when the size of carbon spheres is 500 nm and the content of carbon spheres in the film is 15 wt%, much higher than the 5.6% obtained for pure nanocrystalline films.<sup>37</sup>

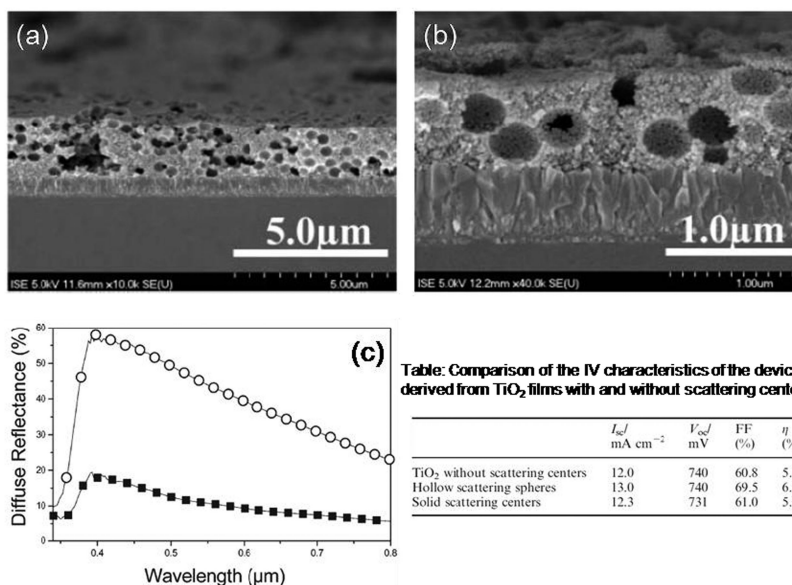


**Fig. 7** Spherical voids used in DSCs as light scatterers: (a) and (b) show SEM images of TiO<sub>2</sub> nanocrystalline film with spherical voids embedded inside; and (c) shows diffuse reflectance spectra of nanocrystalline films without (black square) and with (white circle) spherical void light scatterers.<sup>36</sup>

(3) *Other nanostructures as light scattering centers.* In addition to the large TiO<sub>2</sub> particles and spherical voids mentioned above, some other nanostructures, including TiO<sub>2</sub> nanorods, nanowires,<sup>38,39</sup> and nanotubes,<sup>40,41</sup> as well as other materials such as carbon nanotubes and<sup>42</sup> glass powders<sup>43</sup> have been also studied as light scatterers in DSCs by being embedded into the nanocrystalline film. For one-dimensional nanostructures serving as light scatterers, it has been also emphasized that the one-dimensional nanostructures may bridge the nanoparticles and thus enhance the electron transport within the photoelectrode film.<sup>42,44</sup> However, in view of the high scattering efficiency of spherical scatterers and near-ideal dye adsorption on TiO<sub>2</sub>, as well as highly efficient electron injection between the ruthenium dyes and anatase TiO<sub>2</sub>, those scatterers other than TiO<sub>2</sub> large particles have not produced a more significant enhancement on the solar cell performance, the exception being a new nanostructure called the *nanocrystallite aggregate* which will be discussed later.

(4) *Haze factor.* Haze factor is an important concept that describes the ratio of diffused transmittance to total optical transmittance for a translucent film. The transparency as well as the degree of light scattering of a nanocrystalline film mixed with large particles can be represented by the haze factor. In other words, haze factor may provide a quantitative description of the light scattering ability of a photoelectrode film. Chiba *et al.* systematically studied the dependence of the performance of a DSC on the haze of the photoelectrode film.<sup>45</sup> It was found that, as shown in Fig. 8, in general the IPCE of the cell with a TiO<sub>2</sub> photoelectrode increased as the haze factor of the photoelectrode film was increased. However, the degree of the haze factor affecting the IPCE was very dependent on the wavelength of incident light. The most significant increase was observed in the near-infrared region around the 800 nm wavelength, where the IPCE greatly increased from ~10 to ~50% when the haze was increased from 3% to 76%. In the visible region, with wavelengths from

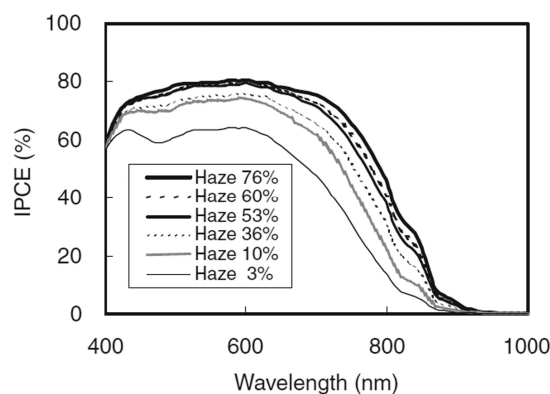


**Fig. 8** Dependence of IPCE spectra on haze factor of TiO<sub>2</sub> photoelectrode films. (The haze factor in the figure was measured at 800 nm.)<sup>45</sup>

400 nm to 600 nm, the IPCE increased quickly, from 65% to 80%, when the haze factor was increased from 3% to 53%, however it almost reached saturation with further increase in the haze factor. Such an observation suggested that an IPCE as high as 80% was relatively easily obtained in the visible region even using the photoelectrode films with medium haze factor because of the extremely large extinction coefficient of the ruthenium dyes to visible light. However, in the near-infrared region, a high haze factor was necessary for the photoelectrode to achieve high IPCE in view of the small extinction coefficient of dyes in this region. In the work of Chiba *et al.*, the highest short-circuit photocurrent density, ~21 mA cm<sup>-2</sup>, was achieved with a TiO<sub>2</sub> photoelectrode with haze factor of 76%, resulting in 11.1% DSC conversion efficiency.<sup>45</sup>

### 3.2.2 Double-layer structure

(1) *Large TiO<sub>2</sub> particles as scattering layer.* The double-layer structure photoelectrode, which is formed by a basic nanocrystalline film and a scattering layer consisting of submicron-sized TiO<sub>2</sub> particles placed on the top of the nanocrystalline film,

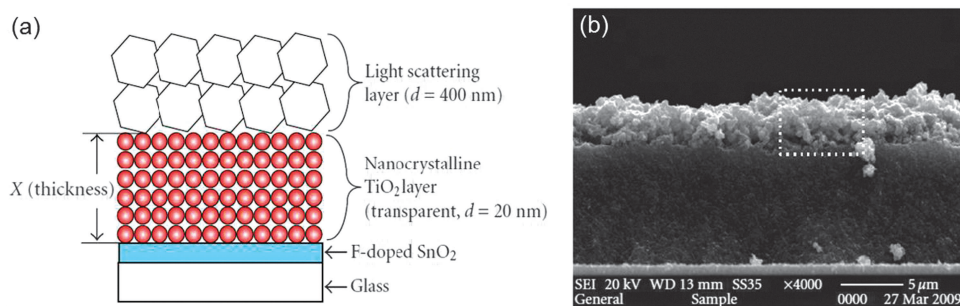


**Fig. 9** Double-layer structure DSC photoelectrode. (a) Schematic drawing of a double-layer structure photoelectrode formed by a nanocrystalline film and a light scattering layer, and (b) a cross-sectional SEM image of the photoelectrode.<sup>47</sup>

has been extensively studied. A typical double-layer structure is shown in Fig. 9a, where the nanocrystalline film with a thickness of 12–14  $\mu\text{m}$  is made of  $\sim 20$  nm  $\text{TiO}_2$  nanocrystallites, and the scattering layer (4–5  $\mu\text{m}$  in thickness) is comprised of 400 nm  $\text{TiO}_2$  particles.<sup>46,47</sup> The photoelectrode with such a double-layer structure has been reported able to increase the photocurrent density of DSCs by up to 80%.<sup>48</sup>

It has been reported in the literature that the large  $\text{TiO}_2$  particles with a rough surface may generate more effective light scattering than those with a smooth surface. For example, cauliflower-like  $\text{TiO}_2$  spheres, which were synthesized by hydrolysis of  $\text{Ti}(\text{OBU})_4$  in the presence of a tri-block copolymer as structural agent, possessed a rather rough surface. When these kind of scatterers were used in DSCs to form a scattering layer, it was demonstrated that the conversion efficiency of 7.36% achieved by the cell with cauliflower-like  $\text{TiO}_2$  spheres was over one percentage higher than that of 6.25% obtained for the cell using smooth scatterers.<sup>32</sup> The improvement was attributed to the more efficient scattering generated by the scatterers with a rough surface. However, it is also likely that the improvement is partially because the scatterers with a rough surface may give rise to a larger surface area than the smooth ones and, can therefore make a greater additional contribution to the optical absorption than the scatterers with a smooth surface.

With the aim to maximally utilize the light scattering effect to enhance solar cell performance, many other studies regarding the optimization of the double-layer structure DSC photoelectrode in terms of scatterer size, layer thickness, and fabrication method have been also reported.<sup>49–53</sup> Aside from the double-layer structure, photoelectrodes with a more sophisticated structure, for example, using multiple scattering layers, have been also investigated to better enhance the optical absorption of DSC photoelectrode.<sup>30,54,55</sup>

(2) *TiO<sub>2</sub> nanotube as scattering layer.*  $\text{TiO}_2$  nanotubes, a type of one-dimensional nanostructure, have been also studied to serve as a scattering layer for light reflection in DSCs. In the work reported by Nakayama *et al.*, the  $\text{TiO}_2$  nanotubes were produced on a titanium foil with an anodization method.<sup>56</sup> The product was collected and dispersed in *tert*-butanol to obtain a suspension of  $\text{TiO}_2$  nanotubes. Electrophoretic deposition (EPD) was then applied to the suspension, enabling the  $\text{TiO}_2$  nanotubes to be built onto the top of nanocrystalline film to form a light scattering layer (Fig. 10a). It was observed that the  $\text{TiO}_2$  nanotubes with a length of several microns and a diameter of  $\sim 20$  nm fabricated on the nanocrystalline film were in random

orientation. By studying the DSC performance of such a double-layer structure photoelectrode using a  $\text{TiO}_2$  nanotube scattering layer and comparing with a photoelectrode using commercial large  $\text{TiO}_2$  particles (SP, Ti Nanoxide-300, Solaronix) for light scattering, it was found that the former that used  $\text{TiO}_2$  nanotubes received a higher incident photon-to-current conversion efficiency (IPCE) than the latter that used large  $\text{TiO}_2$  particles (Fig. 10b), accordingly resulting in an overall conversion efficiency of 7.53% for the former, higher than that of 6.91% for the latter. This work performed by Nakayama *et al.* shows that  $\text{TiO}_2$  nanotubes are likely to be better light scatterers in DSCs than large particles. However, there is a lack of further experiments to identify whether the higher efficiency is due to the  $\text{TiO}_2$  nanotube layer with a more efficient light scattering capability than that of the large particles, or because the nanotubes provide a larger surface area than the large particles and thus leading to greater dye adsorption as well as more optical absorption.

An important issue worth being clarified is how the  $\text{TiO}_2$  nanotubes may generate effective light scattering while considering that both the diameter and length dimensions of the nanotubes are far from being comparable with the light wavelength. The most possible reason is that the existence of grain boundaries in the nanotubes due to the dislocation defects formed during the anodization growth and a consequent thermal treatment converting the  $\text{TiO}_2$  from amorphous to crystalline phase, enabling the formation of large grains or aggregates of small grains of size comparable to the wavelengths of incident light. This hypothesis can be to some extent supported by the fact that bamboo-type morphology has been extensively observed on the  $\text{TiO}_2$  nanotubes produced with an anodization method.<sup>57,58</sup> Another possible mechanism of light scattering in the case of randomly orientated  $\text{TiO}_2$  nanotubes involves the pores (or voids) formed among the nanotubes, which opportunely possess sizes at the light wavelength level. The existence of nanotube bundles may also be one of reasons that contribute to the generation of light scattering.<sup>59</sup>

### 3.2.3 Single-layer photoelectrode films with light scattering capability

(1) *TiO<sub>2</sub> nanotube arrays.* Light scattering-induced enhancement in optical absorption has been also observed on photoelectrodes constructed with one-dimensional nanostructures, for example,  $\text{TiO}_2$  nanotube arrays. A work reported by Zhu *et al.* compared photoelectrodes that were constructed with a  $\text{TiO}_2$  nanoparticle film or a nanotube array, which were the

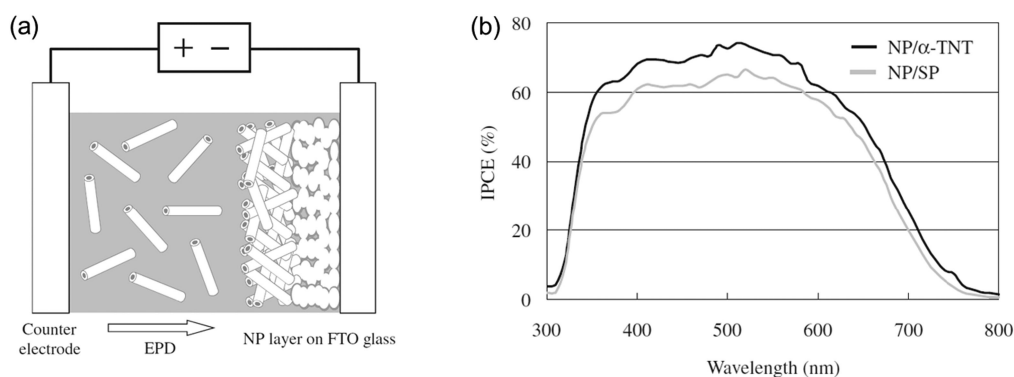


**Fig. 10** TiO<sub>2</sub> nanotubes as light scatterers in DSCs. (a) Preparation of TiO<sub>2</sub> nanotube light scattering layer with an electrophoretic deposition (EPD) method, and (b) a comparison of IPCE of nanocrystalline films using scatterers of commercial TiO<sub>2</sub> particles (referred as NP/SP) or TiO<sub>2</sub> nanotubes (NP/α-TNT).<sup>56</sup>

same in thickness.<sup>60</sup> Besides the advantage of nanotubes that could provide direct pathways for electron transport, which led to a charge recombination in the nanotube array 10 times lower than that in the nanoparticle film, it was found that light harvesting efficiency of the nanotube photoelectrode was at least 20% higher than that of the nanoparticle photoelectrode (Fig. 11). Nakayama *et al.* also studied the DSCs constructed with TiO<sub>2</sub> nanotube arrays, which were produced with an anodization method in an extremely dilute perchloric acid solution, leading to high aspect-ratio nanotubes with a surface area of  $\sim 95 \text{ m}^2 \text{ g}^{-1}$ , equivalent to that of nanoparticles used in conventional DSCs.<sup>61</sup> Characterization of DSC performance of the TiO<sub>2</sub> nanotube array, which was layered 10  $\mu\text{m}$  thick on a Ti substrate, demonstrated an overall conversion efficiency of 5.27%, significantly higher than 3.41% obtained for the nanoparticle film with the same thickness prepared also on a Ti substrate. It was hypothesized that, in addition to the direct pathways provided by the nanotubes for electron transport, the higher efficiency achieved by the nanotube photoelectrode was also a result of higher light harvesting efficiency due to internal light scattering by the nanotubes. The hypothesis is considered to be reasonable in view of the fact that, as we have mentioned above, the TiO<sub>2</sub> nanotubes produced with an anodization method naturally contain a large number of dislocation defects, which lead to the formation of grain boundaries so as to scatter the light. However, no experimental evidence was provided to distinguish the contributions

from the light scattering and the one-dimensional structure of the nanotubes that may transport electrons more efficiently than a nanoparticle film.

(2) *Fibrous network of TiO<sub>2</sub> nanowires.* Although the aforementioned TiO<sub>2</sub> nanotube arrays have been widely studied for DSC applications for their capability to provide direct pathways for electron transport and meanwhile be able to cause light scattering to enhance optical absorption of the solar cells, they are, however, thought to be less-efficient in the generation of light scattering in view of the orientation of the nanotubes parallel to the direction of incident light, making a portion of light pass through the photoelectrode film without being scattered. By employing randomly oriented TiO<sub>2</sub> nanowires, Tetreault *et al.* developed a photoelectrode film with fibrous network structure.<sup>63,64</sup> Although the initial idea of using the randomly oriented TiO<sub>2</sub> nanowires was to achieve a photoelectrode film with a pore size larger than that of a conventional nanocrystalline film so as to meet the need of solid-state DSCs for better infiltration of a gel electrolyte, it was found that the pores formed by the bundles of nanowires as well as the bundles themselves presented dimensions on the scale of the wavelength of light (Fig. 12a) and therefore could cause intensive light scattering in the photoelectrode film, accordingly contributing to the improvement of the optical absorption of the photoelectrode. For a 2.5  $\mu\text{m}$ -thick film comprised of TiO<sub>2</sub> nanowires, approximately 20–40% of visible

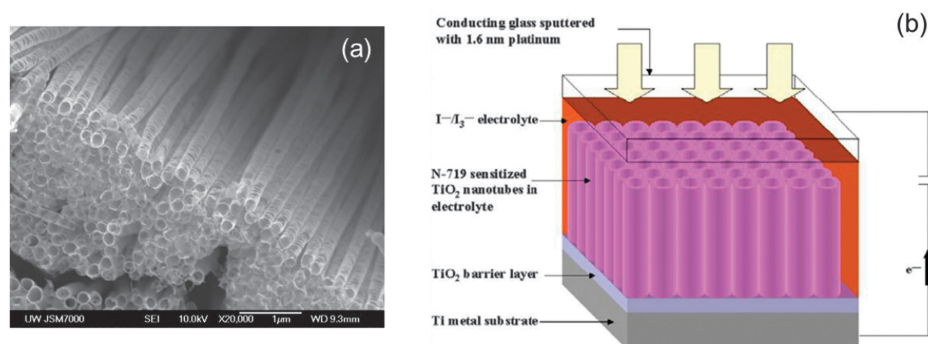


**Fig. 11** DSCs with a TiO<sub>2</sub> nanotube array. (a) SEM image of a TiO<sub>2</sub> nanotube array prepared with an anodic oxidation method, and (b) a schematic drawing of the structure of a DSC with TiO<sub>2</sub> nanotube array fabricated on a Ti metal substrate.<sup>62</sup>

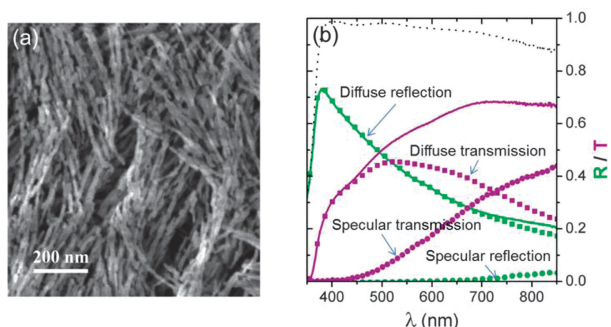


**Fig. 12** Fibrous network structure photoelectrode consisting of TiO<sub>2</sub> nanowires. (a) SEM image, and (b) transmittance and reflectance spectra of the photoelectrode film.<sup>63</sup>

light was found to be scattered by transmission and reflection (Fig. 12b). Besides the merit of being more efficient in light scattering than a nanotube array, the randomly oriented nanowires forming the photoelectrode film of a DSC may also provide benefit in making easier the manufacture of photoelectrodes for DSCs.

(3) *Submicron sized TiO<sub>2</sub> hollow spheres.* Submicron sized TiO<sub>2</sub> hollow spheres are also a structure that can generate highly effective light scattering and, when used in DSCs, they have been reported able to achieve a conversion efficiency comparable to those of conventional photoelectrodes made of a nanocrystalline film.<sup>65</sup> TiO<sub>2</sub> hollow spheres can be prepared with a template method using spherical polystyrene (PS), which is removed in a sequential sintering treatment. The TiO<sub>2</sub> spheres synthesized with this method typically feature a hollow structure with a diameter of 400–500 nm and a shell thickness of 30 nm (Fig. 13). In the work performed by Park *et al.*, the DSC performance of a photoelectrode film consisting of ~12 μm-thick TiO<sub>2</sub> hollow spheres was studied.<sup>65</sup> It was found that the amount of dye adsorbed on the photoelectrode film of TiO<sub>2</sub> hollow spheres was only about one-third of that on a nanocrystalline film, however the DSC conversion efficiency of 4.3% received by the hollow sphere photoelectrode was almost 87% of the 4.95% efficiency obtained for the nanocrystalline film. It was inferred that light scattering generated by the hollow spheres had contributed to the optical absorption and greatly improved the light harvesting efficiency of the photoelectrode.

Multilayered hollow spheres have also been studied for application to DSCs. Compared with single-shelled hollow spheres, the multilayered hollow spheres have the apparent advantage of providing larger specific surface area for dye adsorption.

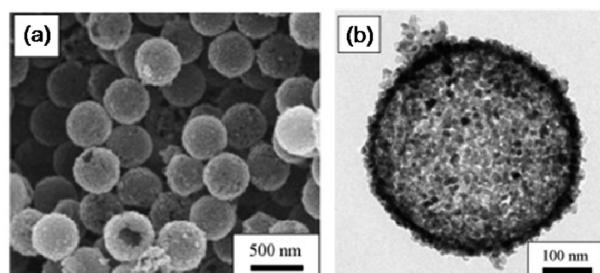


**Fig. 13** TiO<sub>2</sub> hollow spheres. (a) SEM image, and (b) TEM image.<sup>65</sup>

Regarding optical behavior, Qian *et al.*<sup>66</sup> and Wu *et al.*<sup>67</sup> suggested that the multilayered hollow spheres might yield more effective light scattering than the single-shelled hollow spheres due to the existence of multiple layers which led to multiple light scattering and, possibly, optical localization within the spheres. More importantly, in view of the inner spheres having varying sizes, the light scattering could happen in a broader wavelength range than what single-shelled hollow spheres did (Fig. 14). In the work carried out by Qian *et al.*, the DSC with TiO<sub>2</sub>-coated multilayered SnO<sub>2</sub> hollow spheres demonstrated an efficiency of 5.65%, higher than 5.14% obtained for TiO<sub>2</sub> nanocrystalline film (P25) with the same thickness, ~10 μm.<sup>66</sup> In another work reported by Wu *et al.*, multilayered TiO<sub>2</sub> hollow spheres comprising a DSC photoelectrode film did not however show better efficiency than the TiO<sub>2</sub> nanocrystalline film (P25), but their action as a light scattering layer was shown to be able to significantly increase the optical absorption, leading to an impressively high efficiency of ~9.1%.<sup>67</sup> These results verify that the hollow spheres, especially the multilayered hollow spheres, are promising material with light scattering capability for DSC application. However, the structure of them in terms of the size of the spheres and inner cavities, the thickness of each layer, and the number of layers is anticipated to be further optimized to maximize the dye loading and the multiple light scattering effect. A recently published review paper well summarized the existing methods for the synthesis of hollow structured spheres.<sup>68</sup>

(4) *Multifunctional 3D nanostructures.* While light scattering is purposely introduced into DSCs to enhance light harvesting, recently some three-dimensional (3D) nanostructures have been developed to fulfil multiple functions. These 3D nanostructures may not only bring about light scattering, but may also benefit the solar cells by providing other functions, such as offering large internal surface area for sufficient dye loading, or forming an internally connected core-shell structure to reduce the charge recombination in DSCs. Two typical multifunctional 3D nanostructures designed for enhancing the performance of DSCs in these regards are (a) spherical aggregates of oxide nanocrystallites, and (b) host-passivation-guest (H-P-G) structure.

### I. Spherical aggregates of oxide nanocrystallites

(i) *Principle.* As discussed above, large-sized oxide particles have been widely used to generate light scattering in DSCs by

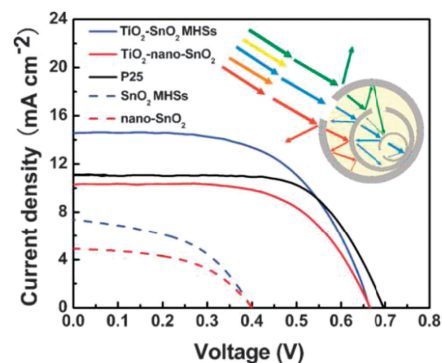


**Fig. 14** TiO<sub>2</sub>-coated SnO<sub>2</sub> multilayered hollow spheres (TiO<sub>2</sub>-SnO<sub>2</sub> MHSs) demonstrating high DSC efficiency. The inset schematically shows multiple light scattering within a multilayered hollow sphere.<sup>66</sup>

either coupling onto nanocrystalline film as a reflecting layer or being mixed into the nanocrystalline film as scattering centers. However, these methods are thought somewhat non-ideal for the reason that in the case of the double-layer structure the light is only reflected once, and in the case of mixture structure the integration of large-sized particles may inevitably lead to a loss in the internal surface area of the photoelectrode film. Therefore there has been a demand for creating a new nanostructure that may form the photoelectrode film with both a large surface area and the capability of generating light scattering. Nanocrystallite aggregates, which were introduced for DSC application for the first time in 2007,<sup>69</sup> are a hierarchical nanostructure that may satisfy the dual requirements of high surface area and light scattering. A nanocrystallite aggregate is a spherical assembly of nano-sized oxide crystallites and possesses a diameter on the submicron scale. Owing to such a structural feature, the photoelectrode film comprised of nanocrystallite aggregates may on one hand provide an internal surface area nearly equal to that of nanocrystalline films in view of the building blocks of nano-sized crystallites forming the aggregates, and on the other hand have the capability of generating light scattering due to the submicron size of the aggregates, which is comparable to the wavelength of visible light.

In the case of a photoelectrode film that is made of nanocrystallite aggregates, the aggregates serve as scatterers causing light scattering within the photoelectrode film. Such light scattering may benefit DSCs by extending the traveling distance of light within the photoelectrode film and thus increasing the probability of photons to interact with the dye molecules adsorbed on the surface of oxide nanocrystallites (Fig. 15).<sup>15,70</sup> This finally leads to an improvement in the optical absorption of the photoelectrode. It is worth pointing out that the light scattering does not happen to a large extent within a nanocrystalline film, for the reason that the size of the nanocrystallites ( $\sim 25$  nm) is far smaller than the wavelength of visible light. Therefore, the propagation of light in a nanocrystalline film occurs along a straight path. As a result, for except the portion being absorbed, the incident light flows through the film and transmits out of the film (Fig. 16). However, one cannot expect to improve the optical absorption of a DSC by simply increasing the thickness of the photoelectrode film for the reason that the thickness of a DSC photoelectrode film

is limited by the electron diffusion length, typically  $\sim 15$ – $20$   $\mu\text{m}$  in nanocrystalline films.<sup>6,71</sup>

(ii) *Example 1: ZnO nanocrystallite aggregates.* ZnO nanocrystallite aggregates were introduced for use in DSCs for the first time in 2007, in an attempt to provide the photoelectrode film with both a large surface area and the capability of generating light scattering.<sup>69</sup> It was reported that the ZnO nanocrystallite aggregates were synthesized through a hydrolysis of zinc acetate dihydrate in diethylene glycol at  $160$   $^{\circ}\text{C}$ .<sup>72,73</sup> In this method, the reaction solution changed to a milky appearance while the temperature approached to  $160$   $^{\circ}\text{C}$ , indicating the agglomeration of nano-sized crystallites which resulted in the formation of large aggregates. The reaction solution was aged at  $160$   $^{\circ}\text{C}$  for several hours, and finally concentrated by a sequential operation of: (1) separating the aggregates from the solvent centrifugally; (2) removing the supernatant; and (3) redispersing the precipitate in ethanol to form a suspension solution. Photoelectrode films were prepared with the as-obtained suspension solution using a drop casting method.<sup>66</sup>

It has been demonstrated that, with the method mentioned above, the size polydispersity of ZnO aggregates was related to the heating rate; a rapid heating led to a broad size distribution of the aggregate. Monodisperse aggregates could be synthesized by purposely adding colloidal ZnO containing nanoparticles ( $\sim 5$  nm in diameter) into the reaction solution when the temperature reached  $130$   $^{\circ}\text{C}$ , at which time the agglomeration of nano-sized crystallites started and the added nanoparticles would induce the formation of monodisperse aggregates.<sup>73</sup>

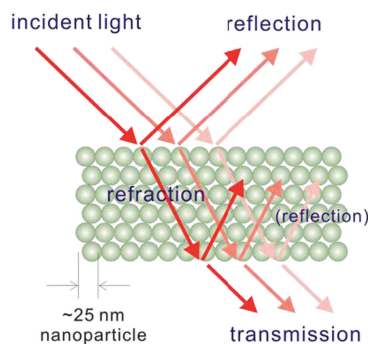


Fig. 16 Light propagation through a nanocrystalline film.

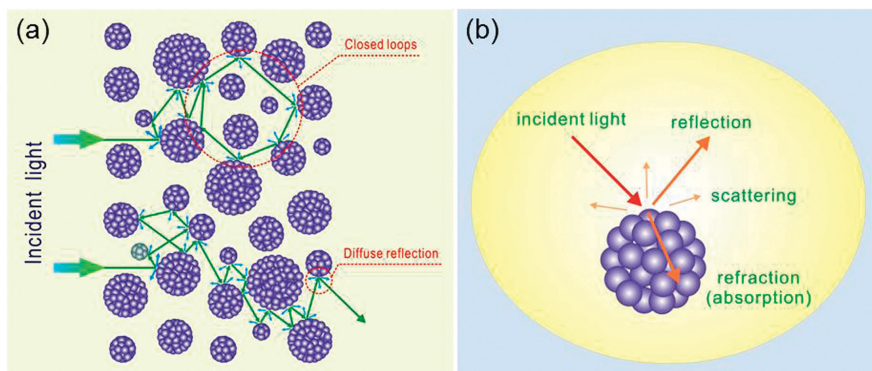
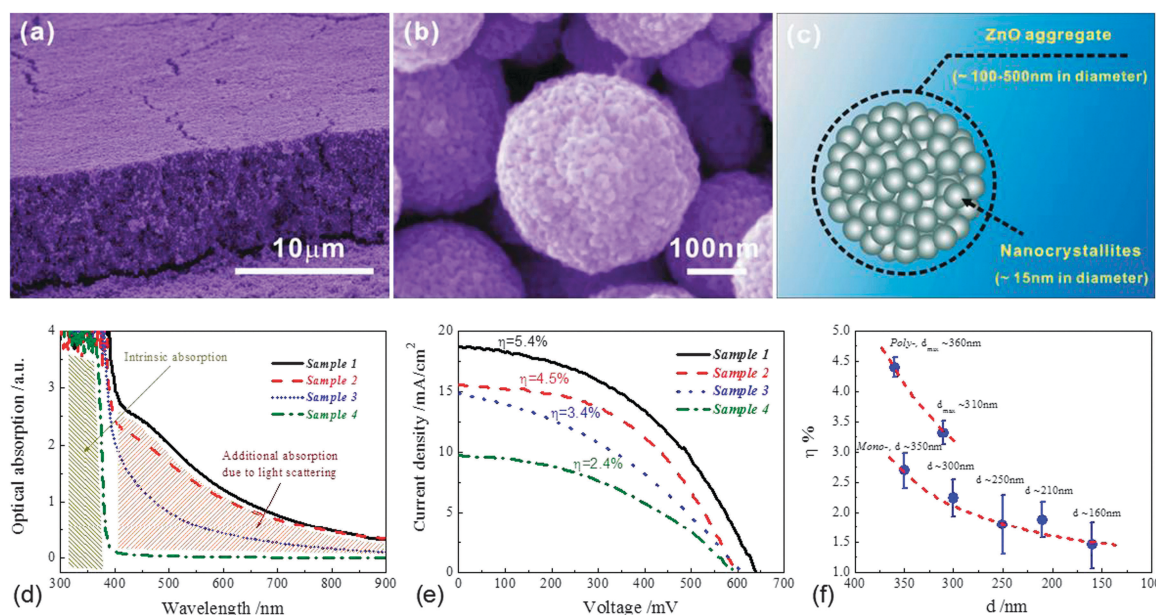


Fig. 15 Schematic drawing of (a) light scattering within a nanocrystallite aggregate film, and (b) optical reflection, refraction and absorption on/inside individual aggregates.<sup>70</sup>



**Fig. 17** Dye-sensitized ZnO solar cells. (a) SEM image of photoelectrode film consisting of ZnO nanocrystallite aggregates, (b) SEM image of individual ZnO nanocrystallite aggregates, (c) schematic drawing of the structure of a ZnO aggregate comprised of nano-sized crystallites, (d) optical absorption spectra and (e)  $I$ - $V$  curves of Samples 1 through 4, and (f) the dependence of efficiency on size and size distribution of aggregates.<sup>15,74</sup>

The size of resultant aggregates could be adjusted by the amount of colloidal ZnO that was added into the reaction solution. Generally, more colloidal ZnO would lead to smaller aggregates.

Scanning electron microscopy (SEM) characterization revealed that the as-synthesized ZnO aggregates were spherical in shape and consisted of closely packed nanocrystallites (Fig. 17). The nanocrystallites that formed the aggregates were only about 15 nm in diameter, making the aggregates, as well as the photoelectrode film comprised of the aggregates, highly porous. A BET measurement demonstrated that the aggregates possessed an approximate specific surface area of  $80 \text{ m}^2 \text{ g}^{-1}$ .<sup>15</sup> Such a large surface area ensured the photoelectrode film consisting of aggregates was able to achieve sufficient dye adsorption. Meanwhile, these ZnO aggregates featured the dimensions in a range from several tens to several hundreds of nanometers, which well overlapped with the wavelengths of visible light. The aggregates were therefore extremely efficient in the generation of light scattering.

The effectiveness of ZnO aggregates in light scattering can be demonstrated by the optical absorption spectra of aggregate films, which present additional absorption in the visible region where the intrinsic absorption of ZnO does not take place (Fig. 17d). It was explained that the presence of such additional absorption was because of the existence of light scattering, which decreased the transmittance of the aggregate films and was shown as “an extra absorption” on the spectra. Shown in Fig. 17d is a comparison between the absorption spectra of three ZnO aggregate films and a ZnO nanocrystalline film. Sample 1 consists of perfect ZnO aggregates, presenting the most intense absorption in the visible region. Sample 4 representing a ZnO nanocrystalline film comprised of nanocrystallites with a size far smaller than the wavelengths of incident light is only observed to have absorption in the near-ultraviolet region, corresponding to the intrinsic absorption of a ZnO semiconductor. The other two samples referred as

Samples 2 and 3 are films formed by ZnO aggregates, however the spherical shape of the aggregates is altered in each case to a different degree. Sample 2 with less alteration presents a higher absorption than Sample 3, due to the stronger light scattering generated by the former than by the latter. Shown in Fig. 17e are  $I$ - $V$  curves of DSCs constructed with Samples 1 through 4. The trend for dependence of solar cell efficiency on the film structure is exactly the same as that for optical absorption. Sample 1 with perfect aggregates receives the highest efficiency,  $\sim 5.4\%$ , while Sample 4 comprised of dispersed nanoparticles achieves the lowest efficiency,  $\sim 2.4\%$ . These results verify that nanocrystallite aggregates forming photoelectrode film generate effective light scattering that improves the optical absorption of the photoelectrode, leading to a significant enhancement in the conversion efficiency of DSCs.

In other research performed by Zhang *et al.*, the DSC performance of ZnO aggregates with different sizes and size distributions was studied.<sup>74</sup> It was found that the aggregates with a size closer to the wavelengths of incident light could result in more intensive light scattering and therefore achieve higher solar cell conversion efficiency (Fig. 17f). More importantly, the aggregates with a broader size distribution and an average size closer to the wavelength of light were observed to have a higher conversion efficiency due to a more effective scattering over a wider range of wavelengths. Additionally, the better packing of different-sized aggregates while forming the photoelectrode film was also suggested to be a reason that further contributed to the improved performance.

Another impressive work with ZnO nanocrystallite aggregates was carried out by Cheng *et al.*, reporting efficiency as high as 5.3% when the aggregate film was sensitized by a metal-free organic indoline dye, coded D205.<sup>75</sup> Through the use of ZnO nanocrystallite aggregates produced with a spray pyrolysis method and adding a ZnO thin film in the photoelectrode film

as buffer layer, a new efficiency record of 7.5% for dye-sensitized ZnO solar cells has been recently achieved by Memarian *et al.*<sup>76</sup>

(iii) *Example 2: TiO<sub>2</sub> aggregates.* TiO<sub>2</sub> nanocrystallite aggregates, the so-called mesoporous beads or nanoporous spheres in the literature, have also been studied recently for use in dye-sensitized solar cells.<sup>65,77–79</sup> In the work performed by Sauvage *et al.*<sup>78</sup> and Chen *et al.*,<sup>77,80</sup> TiO<sub>2</sub> mesoporous beads were fabricated *via* a two-step method in which amorphous TiO<sub>2</sub> beads were synthesized firstly and then a hydrothermal treatment in a solution containing ammonia was applied to the TiO<sub>2</sub> beads to achieve a mesoporous structure. The TiO<sub>2</sub> mesoporous beads produced with this method had a diameter of approximately 830 nm, BET surface area of 89 m<sup>2</sup> g<sup>-1</sup>, and a mean pore size of 23 nm. Sauvage *et al.* compared the IPCE spectra between those of the DSCs with photoelectrode film made of TiO<sub>2</sub> nanoparticles (P25) and TiO<sub>2</sub> mesoporous beads.<sup>78</sup> It was observed that, due to light scattering, the efficiencies of mesoporous bead solar cells were apparently higher than those of nanoparticle solar cells over the entire wavelength range of light (Fig. 18a), resulting in efficiency of 9.1% (note: the efficiency reached 10.6% after TiCl<sub>4</sub> treatment) for TiO<sub>2</sub> mesoporous beads, much higher than the 7.1% (8.5% after TiCl<sub>4</sub> treatment) for the P25 nanoparticles. A further study that normalized the IPCE spectra revealed that the enhancement arising from light scattering was more efficient at the wavelengths above 600 nm than in the region of visible light (Fig. 18b). This was explained by that the dye was able to absorb visible light intensively, however this was insufficient in the long wavelength region, where the light scattering effect was presented, this was helpful for the improvement of the optical absorption by extending the traveling distance of the incident light within the photoelectrode film. A similar phenomenon has been also observed in a work reported by Kim *et al.*, in which nanoporous TiO<sub>2</sub> spheres with a diameter of ~250 nm presented incident-photon-to-current conversion efficiencies higher than 20 nm-sized nanoparticles at long wavelengths ranging from 600 nm to 700 nm.<sup>65</sup>

In addition to generating light scattering, TiO<sub>2</sub> nanocrystallite aggregates used for DSCs have been also reported to have other advantages. For example, the TiO<sub>2</sub> mesoporous

beads synthesized with an etching method were found to be able to provide a more accessible internal surface area than P25 nanoparticles, and therefore the saturation dye adsorption capacity of the former,  $7.12 \times 10^{-5} \text{ mol g}^{-1}$ , is higher than that of  $4.25 \times 10^{-5} \text{ mol g}^{-1}$  for the latter.<sup>77</sup> It was also found that the lifetime of the photoelectrons in a nanocrystallite aggregate film was longer than in the conventional nanocrystalline film, meaning that the electron diffusion length in the aggregate film was longer than in the nanocrystalline film.<sup>78</sup> This was attributed to the closely packed structure of nanocrystallites within the aggregates, which resulted in a decreased charge recombination rate and thus an enhancement in the transport of photogenerated electrons within the photoelectrode film. These advantages of nanocrystallite aggregates plus their light scattering capability have made them a promising nanomaterial for DSCs to achieve high conversion efficiency with single-layer photoelectrode films.

In a recent work reported by Park *et al.*, the TiO<sub>2</sub> nanocrystallite aggregates were adapted to work as light scatterers for double-layer structure DSCs.<sup>81</sup> It is impressive that the light scattering capability of the TiO<sub>2</sub> nanocrystallite aggregates was inferior to that of commercial light scattering TiO<sub>2</sub> particles (Solaronix), however when combined with a nanocrystalline film to serve as a light scattering layer, the former achieved an overall conversion efficiency of 9.37%, greatly higher than that of 8.20% for the latter. A similar phenomenon was also observed in the study performed by Yu *et al.*<sup>82</sup> Such a scenario well demonstrates the superiority of TiO<sub>2</sub> nanocrystallite aggregates, which possess a porous structure and are therefore able to provide a larger specific surface area for more dye loading than the conventional scattering particles. However, considering the fact that the efficiency achieved by the double-layer structure DSCs employing TiO<sub>2</sub> nanocrystallite aggregates for light scattering actually doesn't exceed what is obtained for the photoelectrode comprised of single-layer TiO<sub>2</sub> nanocrystallite aggregates; from the ease-of-manufacture point of view, the single-layer structure photoelectrodes are preferred.

**II. Host-passivation-guest (H-P-G) structure.** The host-passivation-guest (H-P-G) structure was purposely developed by Tetreault *et al.* to meet the needs of solid-state DSCs (SS-DSCs) with large pores for the infiltration of the gel

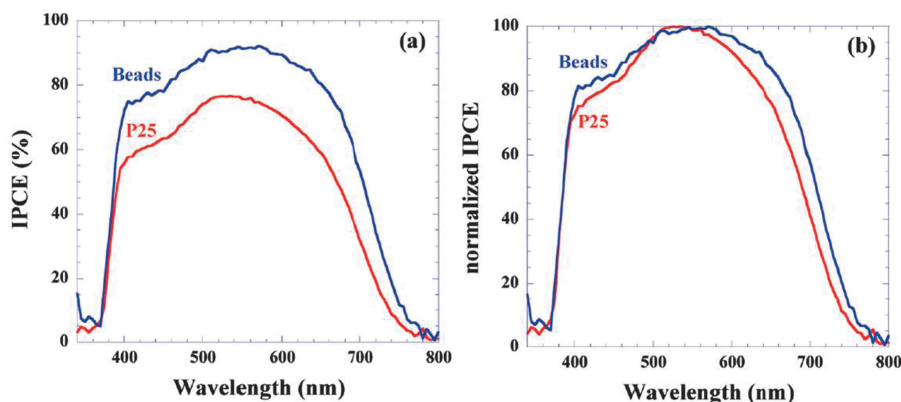


Fig. 18 IPCE spectra of DSCs with photoelectrodes made of P25 nanoparticles and mesoporous TiO<sub>2</sub> beads.<sup>78</sup>

electrolyte and to reduce the charge recombination when employing high-conductivity oxides such as Al-doped ZnO (Al : ZnO) and SnO<sub>2</sub> for photoelectrode.<sup>64,83</sup> Opportunely, the pore size of the H-P-G structure photoelectrode film was on the scale of the wavelength of light, giving the film a strong light scattering capability which benefited the solar cell by enhancing the optical absorption.

The H-P-G structure was synthesized through a use of polystyrene microspheres as template, on which a layer of 90 nm-thick high-conductivity oxide, for example Al : ZnO or SnO<sub>2</sub>, was coated *via* atomic layer deposition (ALD) to serve as the *host* layer. A layer of 25 nm-thick TiO<sub>2</sub> was then deposited to work as the *passivation* layer, that is preventing the electrons in the host layer (SnO<sub>2</sub>) from recombining with the oxidized form of the redox mediator in the electrolyte and meanwhile forming adsorption sites for dye loading. To enhance the internal surface area of the photoelectrode film, TiO<sub>2</sub> nanoparticles were filled into the gaps formed by the microspheres. Finally, the film consisting of core-shell (Al : ZnO@TiO<sub>2</sub> or SnO<sub>2</sub>@TiO<sub>2</sub>) structure spheres and TiO<sub>2</sub> nanoparticles was treated with a TiCl<sub>4</sub> aqueous solution, allowing the formation of a thin layer of TiO<sub>2</sub> as *guest*, which was believed to be able to strengthen the connectivity between the nanoparticles and moreover increase the internal surface area of the photoelectrode film. A consequent thermal treatment at 500 °C for 1 h was carried out to burn off the organic materials from the film, leading to the formation of a 3D porous photoelectrode with the so-called H-P-G structure (Fig. 19).

The most outstanding advantage of the H-P-G structure photoelectrode for DSCs can be demonstrated by the higher open-circuit voltages (~791–842 mV) compared to those for photoelectrodes made of conventional TiO<sub>2</sub> nanocrystalline film. The achievement of high-open circuit voltage has been explained to be a result of the well interconnected core-shell structure spheres that may reduce the charge recombination and thus improve the charge collection capability of the photoelectrode. It is impressive that the SnO<sub>2</sub> serving as the host may produce a short-circuit current of 10.4 mA cm<sup>-2</sup>, significantly higher than the 6.9 mA cm<sup>-2</sup> short-circuit current obtained for the TiO<sub>2</sub> host, firmly implying that the use of high-conductivity oxide core in the H-O-G structure is an effective way of lowering the charge recombination and may accordingly enhance electron transport within a DSC photoelectrode.

In addition to benefiting from the core-shell structure that led to a reduction in the charge recombination, the satisfying photocurrent achieved by H-P-G structure photoelectrodes

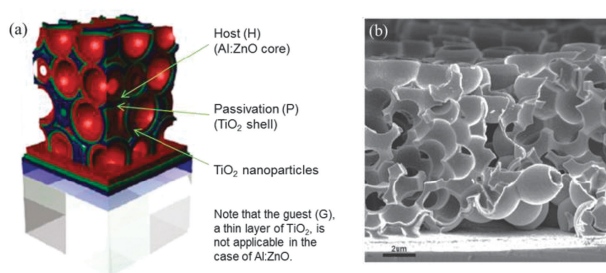


**Fig. 19** (a) Schematic drawing and (b) cross-sectional SEM image of the H-P-G structure photoelectrode.<sup>83</sup>

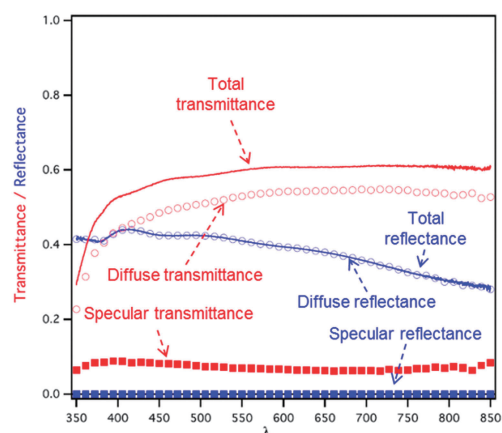


**Fig. 20** Transmittance and reflectance spectra of a TiO<sub>2</sub>-passivated Al : ZnO H-P-G structure photoelectrode film.<sup>84</sup>

was also believed to be partially contributed by the light scattering that enhances the optical absorption of the photoelectrode; in view of the fact that both the hollow core-shell spheres themselves and the pores among the core-shell spheres have dimensions on the scale of the wavelength of light. Shown in Fig. 20 are the transmittance and reflectance spectra of a H-P-G structure photoelectrode comprised of a TiO<sub>2</sub> passivated Al : ZnO host. It can be seen that, compared with specular transmission and reflection, diffuse transmission and reflection present an apparently predominant contribution to the optical behavior of the H-P-G structure film, implying the existence of intensive light scattering in the H-P-G structure photoelectrode film. However, while the H-P-G photoelectrode was purposely developed to create large pores for gel electrolyte infiltration and meanwhile emphasize the reduction of the charge recombination through a core-shell structure, although it may also generate light scattering the internal surface area of this kind of photoelectrode film is thought not to be as large as that of the photoelectrode made of nanocrystallite aggregates (as described in Section 4.1), to great extent limiting the dye adsorption amount and thus diminishing the maximum attainable efficiency.

#### 4. Conclusions and outlook

The above discussion attests that light scattering is an effective approach that can improve the optical absorption of the DSC photoelectrode. In general, relying on the structure of the photoelectrode film, light scattering can be achieved in three ways: (1) a mixed structure containing large particles as light scatterers embedded into a nanocrystalline film (Structure-1) (Fig. 21a); (2) a double layer structure comprised of a basic nanocrystalline film and a scattering layer consisting of large particles placed at the back of the nanocrystalline film for light reflection (Structure-2) (Fig. 21b); and (3) a one layer structure consisting of 3D hierarchical nanostructures, for example, nanocrystallite aggregates (Structure-3) (Fig. 21c), which on one hand possess dimensions comparable to the wavelength of visible light and can therefore generate effective light scattering and, on the other hand, may offer a large specific surface area comparable to that of nanocrystalline film for dye adsorption.

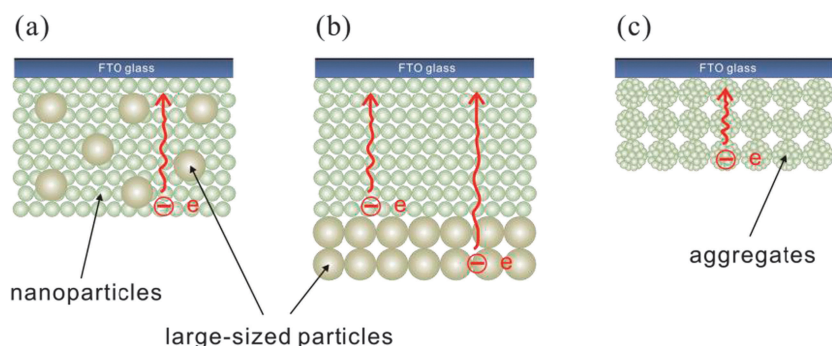


**Fig. 21** Comparison of electron diffusion length in (a) a nanocrystalline film incorporating large-sized particles as light scatterers, (b) a nanocrystalline film coupled with a layer of large-sized particles for light scattering/reflection, and (c) a film consisting of nanocrystallite aggregates.

As we have mentioned, light scattering is introduced into DSCs to increase the optical absorption of the photoelectrode in view of the fact that the maximally allowed thickness of a DSC photoelectrode film is limited by electron diffusion length due to the existence of charge recombination. In other words, one cannot expect to increase optical absorption by boosting the thickness of photoelectrode film, whereas the light scattering is introduced to extend the traveling distance of incident light within the photoelectrode film so as to improve light harvesting of the photoelectrode. However, in the case of Structure-1, the use of large particles as light scatterers mixed into the nanocrystalline film would unavoidably lead to a decrease in the internal surface area of the photoelectrode film. In the case of Structure-2, although the use of an additional scattering layer would not affect the internal surface area of the nanocrystalline film, the incident light is only reflected once and therefore the effect of extending the traveling distance of light is less effective than in Structure-1. Structure-3 is potentially able to overcome the drawbacks in Structure-1 and Structure-2, and is promising in achieving high-efficiency DSCs. In addition to the hierarchical nanostructures comprised of nano-sized building blocks providing an internal surface area comparable to that of nanoparticles and the spherical nanocrystallite aggregates generating very effective light scattering, more importantly, the light scattering of hierarchical nanostructures enables the optical absorption of a photoelectrode film constructed with hierarchical nanostructures to be much more efficient than that of a film comprised of nanoparticles alone. As a result, the photoelectrode film that consists of hierarchical nanostructures would allow its thickness to be smaller than the thickness of nanocrystalline films that are currently used in conventional DSCs. This point is critically important, since it means that the photo-generated electrons in a hierarchically structured photoelectrode film would travel a distance shorter than that in a nanocrystalline film (Fig. 21). Shortening the traveling distance of photogenerated electrons would result in a reduction of the recombination rate in DSCs, leading to enhanced photocurrent and an increase in the solar cell conversion efficiency. In conclusion, the advantage of hierarchically structured photoelectrode films in optical absorption plus the other merits in terms of dye adsorption and charge transport make the hierarchically structured photoelectrode film an extremely promising candidate for achieving high-efficiency DSCs over the existing films.

## Acknowledgements

This work related to the fabrication and characterization of dye-sensitized solar cells is supported by the U.S. Department of Energy, Office of Basic Energy Sciences, Division of Materials Sciences, under Award no. DE-FG02-07ER46467 (Q. F. Z.). The device fabrication and optimization is also supported in part by the National Science Foundation (DMR 1035196), and the Royalty Research Fund (RRF) from the Office of Research at University of Washington.

## Notes and references

- W. Hoffmann, *Sol. Energy Mater. Sol. Cells*, 2006, **90**, 3285–3311.
- M. A. Green, *Phys. E.*, 2002, **14**, 65–70.
- L. T. Dou, J. B. You, J. Yang, C. C. Chen, Y. J. He, S. Murase, T. Moriarty, K. Emery, G. Li and Y. Yang, *Nat. Photonics*, 2012, **6**, 180–185.
- M. Gratzel, *J. Photochem. Photobiol., C*, 2003, **4**, 145–153.
- A. Yella, H. W. Lee, H. N. Tsao, C. Y. Yi, A. K. Chandiran, M. K. Nazeeruddin, E. W. G. Diau, C. Y. Yeh, S. M. Zakeeruddin and M. Gratzel, *Science*, 2011, **334**, 629–634.
- M. Gratzel, *Inorg. Chem.*, 2005, **44**, 6841–6851.
- C. Longo and M. A. De Paoli, *J. Braz. Chem. Soc.*, 2003, **14**, 889–901.
- N. Martsinovich and A. Troisi, *Energy Environ. Sci.*, 2011, **4**, 4473–4495.
- Z. J. Ning, Y. Fu and H. Tian, *Energy Environ. Sci.*, 2010, **3**, 1170–1181.
- Q. F. Zhang and G. Z. Cao, *Nano Today*, 2011, **6**, 91–109.
- Q. F. Zhang, S. Yodyingyong, J. T. Xi, D. Myers and G. Z. Cao, *Nanoscale*, 2012, **4**, 1436–1445.
- Q. F. Zhang, C. S. Dandeneau, K. Park, D. W. Liu, X. Y. Zhou, Y. H. Jeong and G. Z. Cao, *J. Nanophotonics*, 2010, **4**, 041540.
- Q. F. Zhang and G. Z. Cao, *J. Mater. Chem.*, 2011, **21**, 6769–6774.
- Q. F. Zhang, K. Park, J. T. Xi, D. Myers and G. Z. Cao, *Adv. Energy Mater.*, 2011, **1**, 988–1001.
- Q. F. Zhang, T. R. Chou, B. Russo, S. A. Jenekhe and G. Z. Cao, *Angew. Chem., Int. Ed.*, 2008, **47**, 2402–2406.
- Q. F. Zhang, C. S. Dandeneau, X. Y. Zhou and G. Z. Cao, *Adv. Mater.*, 2009, **21**, 4087–4108.
- C. Bohren and D. Huffman, *Absorption and scattering of light by small particles*, John Wiley & Sons, New York, 1983.
- H. Hulst, *Light Scattering by Small Particles*, Dover Publications, New York, 1981.
- M. Kerker, *The Scattering of Light and Other Electromagnetic Radiation*, Academic, New York, 1969.
- H. Holik, *Handbook of Paper and Board*, Wiley-VCH, 2006.
- H. K. Pulker, G. Paesold and E. Ritter, *Appl. Opt.*, 1976, **15**, 2986–2991.
- J. Ferber and J. Luther, *Sol. Energy Mater. Sol. Cells*, 1998, **54**, 265–275.
- A. Usami, *Chem. Phys. Lett.*, 1997, **277**, 105–108.

- 24 X. Bi, Z. Bao, B. Jing, Z. Qing, L. Yan, C. Wei and C. Jun, *Chin. Phys. B*, 2008, **17**, 3713–3719.
- 25 G. Rothenberger, P. Comte and M. Gratzel, *Sol. Energy Mater. Sol. Cells*, 1999, **58**, 321–336.
- 26 F. E. Galvez, E. Kemppainen, H. Miguez and J. Halme, *J. Phys. Chem. C*, 2012, **116**, 11426–11433.
- 27 C. J. Barbe, F. Arendse, P. Comte, M. Jirousek, F. Lenzenmann, V. Shklover and M. Gratzel, *J. Am. Ceram. Soc.*, 1997, **80**, 3157–3171.
- 28 W. E. Vargas and G. A. Niklasson, *Sol. Energy Mater. Sol. Cells*, 2001, **69**, 147–163.
- 29 A. Usami, *Sol. Energy Mater. Sol. Cells*, 2000, **64**, 73–83.
- 30 Z. S. Wang, H. Kawauchi, T. Kashima and H. Arakawa, *Coord. Chem. Rev.*, 2004, **248**, 1381–1389.
- 31 S. H. Kang, J. Y. Kim, H. S. Kim, H. D. Koh, J. S. Lee and Y. E. Sung, *J. Photochem. Photobiol., A*, 2008, **200**, 294–300.
- 32 L. Yang, Y. Lin, J. G. Jia, X. R. Xiao, X. P. Li and X. W. Zhou, *J. Power Sources*, 2008, **182**, 370–376.
- 33 C. H. Li, G. W. Kattawar and P. Yang, *J. Quant. Spectrosc. Radiat. Transfer*, 2004, **89**, 123–131.
- 34 T. Nousiainen and K. Muinonen, *J. Quant. Spectrosc. Radiat. Transfer*, 2007, **106**, 389–397.
- 35 V. Suryanarayanan, K. M. Lee, J. G. Chen and K. C. Ho, *J. Electroanal. Chem.*, 2009, **633**, 146–152.
- 36 S. Hore, P. Nitz, C. Vetter, C. Prah, M. Niggemann and R. Kern, *Chem. Commun.*, 2005, 2011–2013.
- 37 G. T. Yang, J. Zhang, P. Q. Wang, Q. A. Sun, J. Zheng and Y. J. Zhu, *Curr. Appl. Phys.*, 2011, **11**, 376–381.
- 38 B. Tan and Y. Y. Wu, *J. Phys. Chem. B*, 2006, **110**, 15932–15938.
- 39 J. H. Yoon, S. R. Jang, R. Vittal, J. Lee and K. J. Kim, *J. Photochem. Photobiol., A*, 2006, **180**, 184–188.
- 40 C. J. Lin, W. Y. Yu and S. H. Chien, *Appl. Phys. Lett.*, 2007, **91**, 233120.
- 41 Y. T. Ma, Y. A. Lin, X. R. Xiao, X. P. Li and X. W. Zhou, *Chin. Sci. Bull.*, 2005, **50**, 1985–1990.
- 42 K. H. Jung, J. S. Hong, R. Vittal and K. J. Kim, *Chem. Lett.*, 2002, 864–865.
- 43 K. H. Park, H. Li, M. Dhayal, J. W. Lee and H. B. Gu, *J. Nanosci. Nanotechnol.*, 2008, **8**, 5252–5256.
- 44 T. Umeyama and H. Imahori, *Energy Environ. Sci.*, 2008, **1**, 120–133.
- 45 Y. Chiba, A. Islam, Y. Watanabe, R. Komiya, N. Koide and L. Han, *Jpn. J. Appl. Phys.*, 2006, **45**, L638.
- 46 S. Ito, M. Nazeeruddin, P. Liska, P. Comte, R. Charvet, P. Pèchy, M. Jirousek, A. Kay, S. Zakeeruddin and M. Grätzel, *Progr. Photovolt.: Res. Appl.*, 2006, **14**, 589–601.
- 47 S. Ito, M. Nazeeruddin, S. Zakeeruddin, P. Pèchy, P. Comte, M. Grätzel, T. Mizuno, A. Tanaka and T. Koyanagi, *Int. J. Photoenergy*, 2009, **2009**, 517609.
- 48 S. Hore, C. Vetter, R. Kern, H. Smit and A. Hinsch, *Sol. Energy Mater. Sol. Cells*, 2006, **90**, 1176–1188.
- 49 C. P. Hsu, K. M. Lee, J. T. W. Huang, C. Y. Lin, C. H. Lee, L. P. Wang, S. Y. Tsai and K. C. Ho, *Electrochim. Acta*, 2008, **53**, 7514–7522.
- 50 J. T. Jiu, F. M. Wang, M. Sakamoto, J. Takao and M. Adachi, *Sol. Energy Mater. Sol. Cells*, 2005, **87**, 77–86.
- 51 H. J. Koo, J. Park, B. Yoo, K. Yoo, K. Kim and N. G. Park, *Inorg. Chim. Acta*, 2008, **361**, 677–683.
- 52 W. W. Tan, X. Yin, X. M. Zhou, J. B. Zhang, X. R. Xiao and Y. Lin, *Electrochim. Acta*, 2009, **54**, 4467–4472.
- 53 Z. P. Zhang, S. Ito, B. O'Regan, D. B. Kuang, S. M. Zakeeruddin, P. Liska, R. Charvet, P. Comte, M. K. Nazeeruddin, P. Pèchy, R. Humphry-Baker, T. Koyanagi, T. Mizuno and M. Gratzel, *Z. Phys. Chem.*, 2007, **221**, 319–327.
- 54 L. H. Hu, S. Y. Dai, J. Weng, S. F. Xiao, Y. F. Sui, Y. Huang, S. H. Chen, F. T. Kong, X. Pan, L. Y. Liang and K. J. Wang, *J. Phys. Chem. B*, 2007, **111**, 358–362.
- 55 Z. P. Tian, H. M. Tian, X. Y. Wang, S. K. Yuan, J. Y. Zhang, X. B. Zhang, T. Yu and Z. G. Zou, *Appl. Phys. Lett.*, 2009, **94**, 031905.
- 56 K. Nakayama, T. Kubo and Y. Nishikitani, *Jpn. J. Appl. Phys.*, 2008, **47**, 6610–6614.
- 57 L. D. Sun, S. Zhang, X. W. Sun and X. D. He, *J. Nanosci. Nanotechnol.*, 2010, **10**, 4551–4561.
- 58 J. R. Jennings, A. Ghicov, L. M. Peter, P. Schmuki and A. B. Walker, *J. Am. Chem. Soc.*, 2008, **130**, 13364–13372.
- 59 Y. Chen, H. H. Lu, X. M. Wang and S. S. Lu, *J. Mater. Chem.*, 2012, **22**, 5921–5923.
- 60 K. Zhu, N. R. Neale, A. Miedaner and A. J. Frank, *Nano Lett.*, 2007, **7**, 69–74.
- 61 K. Nakayama, T. Kubo and Y. Nishikitani, *Appl. Phys. Express*, 2008, **1**, 112301.
- 62 K. Shankar, G. K. Mor, H. E. Prakasam, S. Yoriya, M. Paulose, O. K. Varghese and C. A. Grimes, *Nanotechnology*, 2007, **18**, 065707.
- 63 N. Tetreault, E. Horvath, T. Moehl, J. Brillet, R. Smajda, S. Bungener, N. Cai, P. Wang, S. M. Zakeeruddin, L. Forro, A. Magrez and M. Gratzel, *ACS Nano*, 2010, **4**, 7644–7650.
- 64 N. Tetreault and M. Gratzel, *Energy Environ. Sci.*, 2012, **5**, 8506.
- 65 Y. J. Kim, M. H. Lee, H. J. Kim, G. Lim, Y. S. Choi, N. G. Park, K. Kim and W. I. Lee, *Adv. Mater.*, 2009, **21**, 3668–3673.
- 66 J. F. Qian, P. Liu, Y. Xiao, Y. Jiang, Y. L. Cao, X. P. Ai and H. X. Yang, *Adv. Mater.*, 2009, **21**, 3663–3667.
- 67 X. Wu, G. Q. Lu and L. Z. Wang, *Energy Environ. Sci.*, 2011, **4**, 3565–3572.
- 68 X. Y. Lai, J. E. Halpert and D. Wang, *Energy Environ. Sci.*, 2012, **5**, 5604–5618.
- 69 T. P. Chou, Q. F. Zhang, G. E. Fryxell and G. Z. Cao, *Adv. Mater.*, 2007, **19**, 2588–2592.
- 70 G. Cao, *Photonics Spectra*, 2008, **42**, 60–61.
- 71 M. Gratzel, *J. Photochem. Photobiol., A*, 2004, **164**, 3–14.
- 72 D. Jezequel, J. Guenot, N. Jouini and F. Fievet, *J. Mater. Res.*, 1995, **10**, 77–83.
- 73 E. W. Seelig, B. Tang, A. Yamilov, H. Cao and R. P. H. Chang, *Mater. Chem. Phys.*, 2003, **80**, 257–263.
- 74 Q. F. Zhang, T. P. Chou, B. Russo, S. A. Jenekhe and G. Cao, *Adv. Funct. Mater.*, 2008, **18**, 1654–1660.
- 75 H. M. Cheng and W. F. Hsieh, *Energy Environ. Sci.*, 2010, **3**, 442–447.
- 76 N. Memarian, I. Concina, A. Braga, S. M. Rozati, A. Vomiero and G. Sberveglieri, *Angew. Chem., Int. Ed.*, 2011, **50**, 12321–12325.
- 77 D. H. Chen, F. Z. Huang, Y. B. Cheng and R. A. Caruso, *Adv. Mater.*, 2009, **21**, 2206–2210.
- 78 F. Sauvage, D. H. Chen, P. Comte, F. Z. Huang, L. P. Heiniger, Y. B. Cheng, R. A. Caruso and M. Gratzel, *ACS Nano*, 2010, **4**, 4420–4425.
- 79 M. Nedelcu, S. Guldin, M. C. Orilall, J. Lee, S. Huttner, E. J. W. Crossland, S. C. Warren, C. Ducati, P. R. Laity, D. Eder, U. Wiesner, U. Steiner and H. J. Snaith, *J. Mater. Chem.*, 2010, **20**, 1261–1268.
- 80 D. H. Chen, L. Cao, F. Z. Huang, P. Imperia, Y. B. Cheng and R. A. Caruso, *J. Am. Chem. Soc.*, 2010, **132**, 4438–4444.
- 81 Y. C. Park, Y. J. Chang, B. G. Kum, E. H. Kong, J. Y. Son, Y. S. Kwon, T. Park and H. M. Jang, *J. Mater. Chem.*, 2011, **21**, 9582–9586.
- 82 I. G. Yu, Y. J. Kim, H. J. Kim, C. Lee and W. I. Lee, *J. Mater. Chem.*, 2011, **21**, 532–538.
- 83 N. Tetreault, E. Arsenaault, L. P. Heiniger, N. Soheilnia, J. Brillet, T. Moehl, S. Zakeeruddin, G. A. Ozin and M. Gratzel, *Nano Lett.*, 2011, **11**, 4579–4584.
- 84 N. Tetreault, E. Arsenaault, L. P. Heiniger, N. Soheilnia, J. Brillet, T. Moehl, S. Zakeeruddin, G. A. Ozin and M. Gratzel, *Nano Lett.*, 2011, **11**, 4579–4584 (ESI).